Associations of Battery Cell Voltage Consistency with Driving Behavior of Real-world Electric Vehicles

Journal Pre-proof

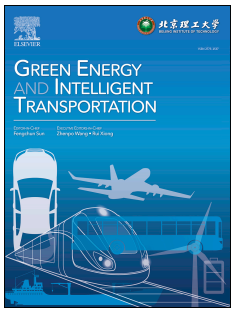

Associations of Battery Cell Voltage Consistency with Driving Behavior of Real-world Electric Vehicles

Shaopeng Li, Hui Zhang, Naikan Ding, Matteo Acquarone, Federico Miretti, Daniela Anna Misul

PII: S2773-1537(24)00088-4

DOI: https://doi.org/10.1016/j.geits.2024.100236

Reference: GEITS 100236

To appear in: *Green Energy and Intelligent Transportation*

Received Date: 30 January 2024

Revised Date: 6 May 2024

Accepted Date: 8 May 2024

Please cite this article as: Li S, Zhang H, Ding N, Acquarone M, Miretti F, Misul DA, Associations of Battery Cell Voltage Consistency with Driving Behavior of Real-world Electric Vehicles, *Green Energy and Intelligent Transportation*, https://doi.org/10.1016/j.geits.2024.100236.

Associations of Battery Cell Voltage Consistency with Driving Behavior of Real-world Electric Vehicles

Shaopeng Li [a, b, c], Hui Zhang [a, b, *], Naikan Ding [a, b], Matteo Acquarone [c], Federico Miretti [c], Daniela Anna Misul [c]

[a] Intelligent Transportation Systems Research Center, Wuhan University of Technology, Wuhan 430063, Hubei, China

[b] Engineering Research Center of Transportation Information and Safety, Ministry of Education, Wuhan University of Technology, Wuhan 430063, Hubei, China

[c] Department of Energy (DENERG) and Center for Automotive Research and Sustainable Mobility (CARS@Polito), Politecnico di Torino, 10138 Torino, Italy

CRediT authorship contribution statement

Shaopeng Li: Conceptualization, Methodology, Software, Formal analysis, Writing - original draft. **Hui Zhang:** Funding acquisition, Supervision, Investigation, Writing - original draft. **Naikan Ding:** Visualization, Project administration, Data curation, Writing - review & editing. **Matteo Acquarone:** Validation, Formal analysis, Writing - review & editing. **Federico Miretti:** Conceptualization, Formal analysis, Writing - review & editing. **Daniela Anna Misul:** Supervision, Conceptualization, Writing - review & editing.

Declaration of competing interest

The authors declare that they have no known competing financial interests or personal relationships that could have appeared to influence the work reported in this paper.

Acknowledgment

This research is sponsored by the Chinese Scholarship Council, and supported by the National Key R&D Program of China (2023YFC3009703) and the National Natural Science Foundation of China (52372341).

GRAPHICAL ABSTRACT

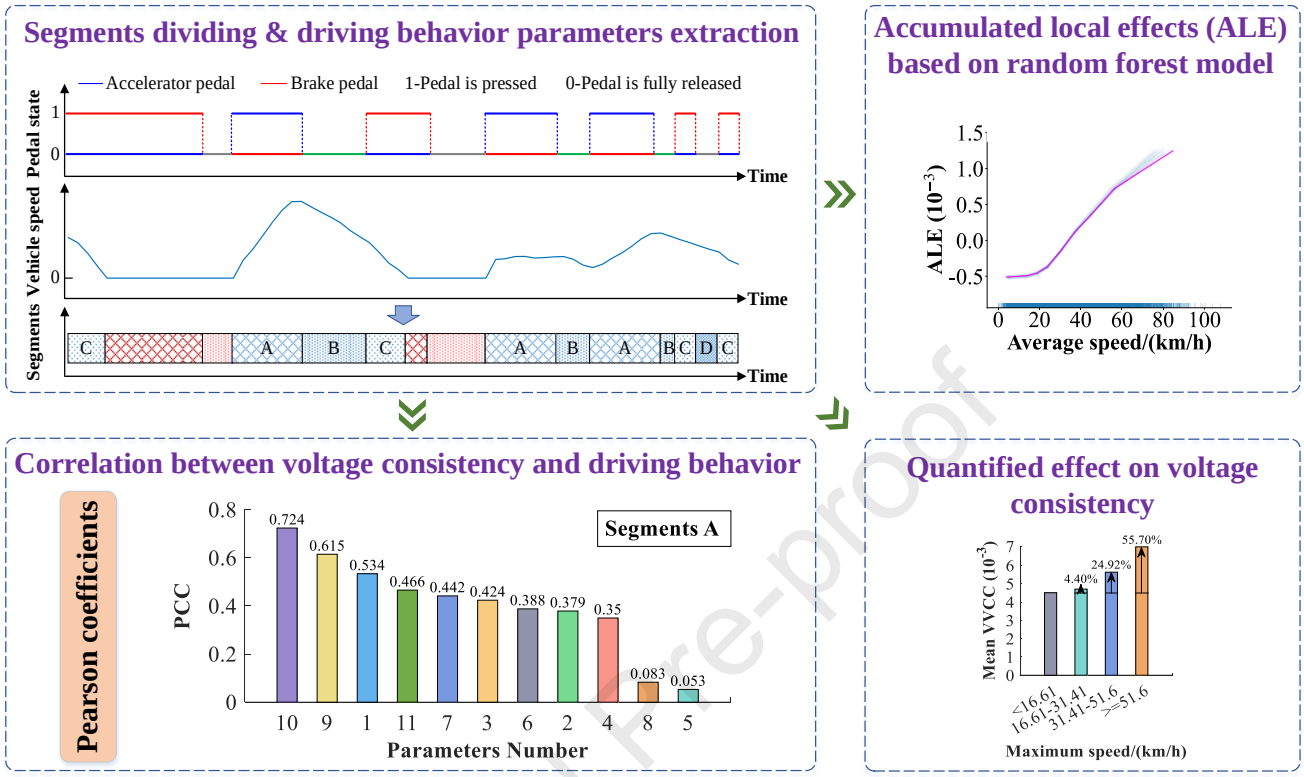

Associations of Battery Cell Voltage Consistency with Driving Behavior of Real-world Electric Vehicles

Abstract: For proposing an adaptive-threshold-based method for detecting battery voltage inconsistency fault, this study explored the associations between driving behavior and voltage consistency between cells (VCC) at a microscopic level, by performing a naturalistic driving experiment on real-world electric vehicles (EVs). The running process of EVs is divided into four kinds of micro-segments A, B, C, D through the driver's pedal actions. Focusing on these segments, Pearson correlation coefficients (PCCs) between driving behavior parameters (DBPs) and voltage variation coefficient between cells (VVCC) are calculated, the impact patterns of DBPs to VVCC are analyzed by accumulated local effects (ALE) plots obtained from random forest (RF) modeling. The results show that the maximum PCC is reached by average accelerator pedal stroke with 0.724 for segments A, and by average speed with 0.789, 0.554, and 0.553 for the other three segments. The four RF models show a high accuracy of VVCC prediction with goodness of fit over 0.919, and the ALE plots demonstrate the impact patterns are positive-nonlinear overall. The maximum VVCC growing rates are reached by average accelerator pedal stroke for segments A (48.09%), and average speed for other segments (55.70%, 29.01%, and 23.68% for segments B, C, and D, respectively). These results imply a strong connection between driving behavior and battery voltage consistency, which could be effectively captured to provide crucial inputs and interpretation methods for modeling voltage consistency prediction during EVs running. Hence, this work lays the foundation for the development of battery voltage fault detection algorithms considering different driving states.

Keywords: Electric vehicles; Driving behavior; Voltage consistency; Association; Random forest

1. Introduction

With the rapid development of electric vehicles (EVs), there is a growing concern about the safety issues of their traction batteries[1-3]. In order to meet the driving power demand and obtain the desired vehicle range, hundreds or even thousands of cells are connected in a series-parallel structure within a battery pack[4-6]. Unfortunately, the inevitable heterogeneity between battery cells is a key factor that influences the performance and safety of the entire battery system[7,8]. A degree of inconsistency, also known as cell-to-cell variation, between cells always exists within the battery pack and cannot be completely avoided. The heterogeneity between battery cells is generally caused by the manufacturing process and can be further exasperated during vehicle usage[9,10]. Indeed, in battery manufacturing, the inevitable minor errors and deviations on electrode fabrication, assembly and formation lead to discrepancies in initial capacity, internal resistance, open-circuit voltage, self-discharge rate and so forth, even for the same batch of battery cells[11,12]. The discrepancies in these initial parameters would cause cell differences in current, voltage, and temperature during long-time real-world operation[13]. Moreover, the nonuniform current and temperature would further aggravate cell inconsistency, which can be embodied by the cell-to-cell variations in depth of discharge, state of charge (SOC), temperature, terminal voltage, output power, capacity, and other factors[14]. An excessive inconsistency between cells must be avoided since it can lead to the issues of over-voltage, under-voltage, over-temperature and even thermal runaway[15-17]. Therefore, a large cell inconsistency is typically classified as a fault because it shows that the battery pack contains overly aged or defective cells[18,19]. Accurate evaluation and diagnosis for inconsistency in the battery pack are necessary to detect aging or faulty cells timely and then prevent thermal runaway.

Many efforts have been dedicated to cell inconsistency evaluation and diagnosis for battery pack in EVs, and various methods have been proposed. These methods can be generally classified into three categories, i.e., signal-

processing-based, model-based and information-fusion-based methods[20]. Signal-processing-based methods generally conduct time-domain or frequency-domain analyses on waveform and amplitude of measured signals, such as voltage, current, and temperature. For time-domain analyses, the quantities such as mean, standard deviation (SD), range, and other statistical descriptors can be used to detect faults[21,22]. Model-based methods obtain cell inconsistency information through the estimation of battery parameters, relying on battery electrochemical models or equivalent circuit models (ECMs)[23]. Electrochemical models have the highest accuracy but also have the highest computational cost and parametrization burden, as a large number of physical parameters must be identified from carefully designed experiments. ECMs offer a compromise as they still provide accurate and physically-interpretable variables while being computationally simple with parameters relatively easy to be estimated[24]. On the other hand, information-fusion-based methods can perform cell inconsistency evaluation and diagnosis by combining information from multi sensors to obtain the best possible fault feature through intelligent algorithms, e.g., weighting/voting fusion[20], clustering algorithm[25], artificial neural network (ANN)[26]. It is worth noting that ANN has been increasingly applied to the estimation and prediction of battery voltage, SOC, and other parameters to improve battery safety and energy efficiency. In particular, powerful deep learning algorithms have shown tremendous potentials and advantages. For example, Lu et al.[27] utilized long short-term memory network (LSTM) to establish a voltage prediction model that could integrate future cyclic conditions and a battery model. Liu et al.[28] estimated battery aging life using bidirectional gated recurrent unit network. Zhang et al.[29] proposed a robust state of health estimation method based on temporal convolutional network (TCN). The ANN is a data-driven approach that can learn hidden relationships between battery states and features without relying on precise expert knowledge or internal mechanisms of battery[30]. Compared to model-based methods that are susceptible to model uncertainty and noise, the ANN based methods usually exhibit stronger robustness in the application on actual EVs.

For real-world EVs, real-time monitoring of battery internal parameters is a challenging task[31]. Many works about cell inconsistency evaluation and diagnosis focus on terminal voltage which has a strong sensitivity to battery working state and can be easily measured and immediately extracted[21]. Poor voltage consistency between cells (VCC) implies the occurrence of voltage abnormity which can lead to one or more battery faults, such as internal short circuit, or electrode structure fault[32]. While battery management systems can monitor and control battery states for well-balanced and fresh cells, managing the voltage of excessively aged or faulty cells is challenging. Hence, excessive voltage inconsistency should be readily detected. For terminal voltage inconsistency evaluation and diagnosis, one of the most common methods is comparing the measured features such as voltage range, SD, variation coefficient, curve distance, and entropy among all cells, with a threshold to determine the alarm level[33]. For instance, Wang et al.[34] adopted the average distance of the voltage curves of all cells as the VCC indicator. On the other hand, Qiu et al.[35] evaluated the voltage inconsistency in battery system using Shannon entropy. Once the difference between the maximum theoretical entropy and the measured entropy of all cell voltages in a certain module or cluster exceeded the preset threshold, the alarm of inconsistency would be triggered. Li et al.[36] employed the correlation coefficient between two cell voltages to measure the cell consistency, and preset a threshold of 0.75 for anomaly detection. Lu et al.[37] calculated the voltage variation coefficient between cells (VVCC) to evaluate the VCC, and the threshold of 0.025 was set to detect the inconsistency at severest level. Li et al.[25] evaluated the deviation of a cell by calculating the difference between its voltage and the average voltage of all cells. If the absolute difference exceeded the 0.1 V threshold, the deviation of the cell was considered to be abnormal. Li et al.[38] proposed an evaluation method for voltage consistency of lithium-ion battery packs in EVs based on the Mahalanobis-Taguchi system, and the first and second-level warning thresholds were set to examine the consistency features extracted through sample entropy and fast-dynamic time warping. Recently, Liu et al.[39] conducted fault diagnosis and type identification of cell voltage inconsistency in electric vehicles using weighted Euclidean distance evaluation, and they set the threshold of evaluation coefficient at 3 in their work. Hence, the cell

with the evaluation coefficient beyond 3 would be detected as a voltage dynamic inconsistency fault. However, in these works, the threshold was set by a fixed value, which may lead to a high false alarm or missed alarm rate. A threshold set too high might lead to a low fault sensitivity, potentially causing the abnormity signal to not trigger the alarm. Conversely, setting it too low could result in normal signals triggering false alarms. Therefore, selecting an appropriate threshold is crucial for fault diagnosis but requires extensive historical fault data for rule establishment, which is difficult in practice[40]. Li et al.[41] analyzed the voltage mean range for fast charging, slow charging, and driving, they found that the boundary line for normal and unsafe battery was significantly different between charging and driving. Therefore, they suggested that different methods or thresholds should be designed for different EV states. To tackle this challenge, Liu et al.[42] proposed online diagnosis and prediction methods for voltage inconsistency fluctuation faults using the SD and improved Pearson correlation coefficient (PCC) as two-dimensional fault features. They selected different thresholds for detecting sudden and progressive voltage fault. Generally speaking, for actual EVs operations, the cell voltages and the measured consistency value fluctuate along with driving status, e.g., a more aggressive driving leads to a more significant voltage variation. Therefore, the threshold should be set accounting for the driving state of EVs.

Few studies have proposed differentiated thresholds for different operation modes or driving states to quantify voltage inconsistency or detect cell voltage abnormity. For instance, Fang et al.[18] set the abnormity threshold of voltage range for three scenarios, i.e., driving, charging, and starting after static charging. In our previous work[43], we set the abnormity threshold of the voltage difference between a cell and the mean cell for four driving behavior modes, and achieved a more accurate detection for cell voltage fault. However, these studies have merely set fixed thresholds for different vehicle operating or driving modes, without quantitatively correlating the battery voltage signal with specific driving conditions. Hence, these thresholds are neither individualized enough nor adjusted adaptively and intelligently in real time according to the specific driving condition. Driving conditions can be assessed using driving state parameters which quantify physical quantities related to driving behaviors. Zhang et al.[44] compared the residuals between the estimated and measured battery voltages using an adaptive threshold to detect the occurrence of internal short-circuit faults. They achieved the dynamical threshold adjustment to variation in environmental factors and driving behavior by using a Gaussian process regression model. In that work, although the voltage consistency was shown to vary with driving behavior and environmental conditions, their relationships were not analyzed.

As previously mentioned, the driver's driving behavior during EV operation would directly impact the fluctuations of battery voltage, current and power. Therefore, to propose an adaptive-threshold-based voltage inconsistency evaluation and diagnosis method, the associations between driving behavior and VCC need to be revealed. So far, a few works have analyzed the correlation between battery voltage and driving factors, but have not established models to reveal the underlying relationship between them. For example, Huang et al.[45] conducted the voltage prediction on fuel cell for the electric bus. In their work, the PCC, Spearman's correlation coefficient, and Kendall's correlation coefficient were utilized to analyze the correlation between voltage and relevant factors during start-stop driving states. However, they did not perform a detailed analysis on the specific fluctuation patterns of voltage along with vehicle speed. Similarly, Zhao et al.[46] adopted PCC in their studies on voltage prediction and inconsistency prognosis to analyze the correlation between vehicle speed and voltage, and found a significant influence of the driving behavior. However, they did not develop a regression model to explore the mapping relationship between driving behavior parameters and the SD of voltage, so only SD of voltage was employed to characterize inconsistency. Few scholars have developed voltage prediction and anomaly detection models based on the analysis of the correlation between driving behavior and battery voltage. For example, Hong et al.[47] adopted the PCC to extract factors strongly correlated with battery voltage, then the vehicle speed and brake pedal stroke were selected as two of the inputs of voltage prediction model. Li et al.[48] also utilized PCC to analyze the

correlation between voltage and variables such as vehicle speed, accelerator pedal stroke, and brake pedal stroke, for constructing a voltage prediction model based on LSTM. The data used in these studies were collected from the platform of National Monitoring and Management Center for New Energy Vehicles in China, its sampling interval is from 10 to 30 s. However, the calculation for VCC indicators such as correlation coefficient, variation coefficient, and entropy must be performed using the continuous data within a time window, namely, data block. Due to the incomplete information of driving behavior caused by large sampling interval within the time window, these studies could not effectively establish a connection between driving behavior and VCC. Consequently, they were unable to deeply analyze the impact mechanisms and practical effects of driving behavior on VCC.

To fill the research gaps mentioned above, this paper conducts naturalistic driving experiments on EVs to investigate the associations between driving behavior and VCC. The detailed study framework is summarized as follows. First, the running process of EVs is divided into four types of segments based on the driving behavior of pressing/releasing pedal, and the driving behavior parameters (DBPs) are extracted for each segment. Then, the PCCs between DBPs and VVCC are calculated and analyzed. Next, a random forest (RF) regression model is established for each type of segments, and the relationship between DBPs and VVCC is assessed using the method of accumulated local effects (ALE). Finally, through data grouping and statistics, the quantitative effects of these important DBPs on VVCC are obtained and investigated.

In summary, the main contributions and innovations of this paper are: 1) For the first time, the association between driving behavior and VCC is investigated using high-frequency running data collected from naturalistic driving experiment on EVs. The challenges arising from low data frequency and incomplete driving behavior information which have previously hindered conducting association analysis, are addressed in this study. 2) A method of dividing the driving phase in different driving segments is proposed to easily capture the association characteristics between the driving behavior and voltage consistency. 3) The association characteristics of correlation, impact pattern, and quantified effect are assessed for a large volume of segments data. Hence, compared with previous works that can hardly obtain the impact mechanisms and practical effects of driving behavior on VCC, this study can directly guide the development of adaptive threshold-based method for voltage inconsistency evaluation and diagnosis. Based on the results in this study, the most significant DBPs for voltage inconsistency prediction modeling can be identified and more insights including impact pattern and nonlinear relationship can be highlighted to enhance model interpretability.

The remainder of this paper is organized as follows. Section 2 introduces the naturalistic driving experiment of EVs, the collected data and their preprocessing process. Section 3 describes EVs running segment division and DBPs extraction method, indicator of VCC, and modeling approach used for analysis. Research results and discussion are then presented in Section 4, followed by the key conclusions summarized in Section 5.

2. Experiment and data acquisition

2.1 Naturalistic driving experiment on EVs

In response to the aforementioned shortcomings in the existing literature, this study designs and conducts naturalistic driving experiment to collect the high-quality vehicular operation data of real-world EVs. The basic requirements for this experiment are that the driving behavior and vehicle running environment during experiment should not be constrained, and the experiment duration should be long enough to obtain a large volume of data in order to account for various running and climate conditions. Considering the above experimental requirements and actual costs, we decided performing the experiment on 20 electric taxies of same specification, driven by 20 professional drivers. The main parameters of the studied vehicles are shown in Table 1. It is noteworthy that the

experimental vehicle's battery pack consists of 24 modules and 192 battery cells, as illustrated in Fig. 1. Each module comprises eight battery cells, with a 2s4p configuration.

Table 1 Specifications of the experimental vehicles

Specifications	Values
Battery type	Ternary lithium-ion
Number of battery cells	96
Number of battery temperature probes	48
Total energy of battery pack	49 kWh
Rated voltage of battery pack	350.4 V
Nominal voltage of battery cell	3.65 V
Rated motor power	42 kW
Rated motor torque	60 Nm

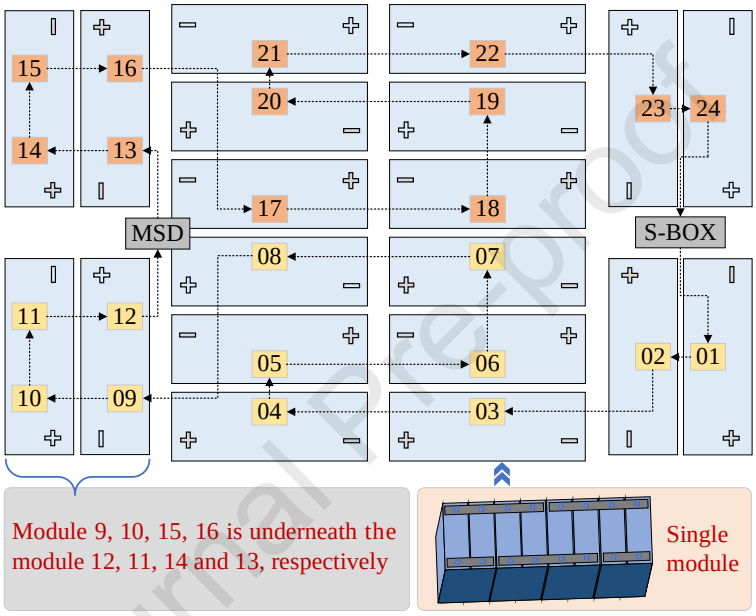

Fig.1 Cells layout inside the battery pack of the studied vehicle

The device of advanced driving assistant system (ADAS) was customized to collect high-frequency data transmitted from controller area network (CAN) of the experimental vehicle, including battery state, ambient temperature, driving state, etc. Those data are stored in the recorder of ADAS along with the data of traffic environment and car following behavior obtained by ADAS camera. The experimental vehicle and data acquisition equipment are shown in Fig. 2.

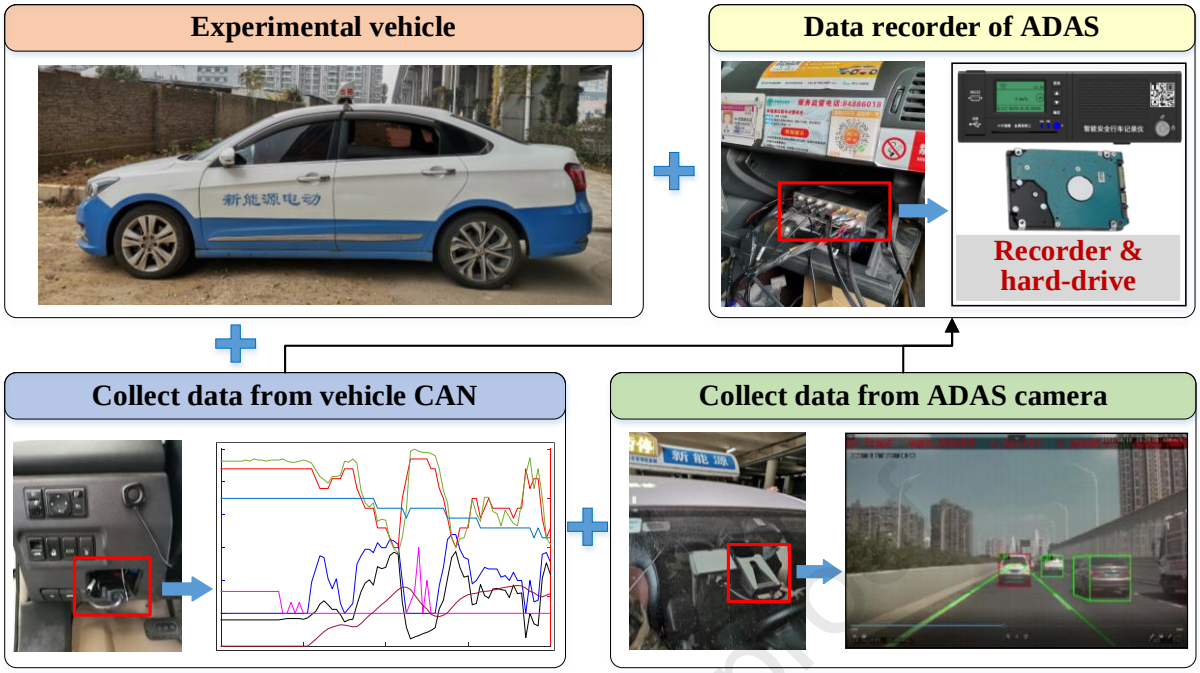

Fig. 2 Experimental data collection process and equipment

This experiment was performed over a period of 10 months from January 28, 2022, to November 28, 2022, within the city of Wuhan, China. This long-duration experiment ensured a wide range of climatic conditions and considerable running scenarios within which EVs operated. Throughout the experiment, there were no limitations imposed on driving time or routes. In essence, the operation of the EVs remained entirely unconstrained in Wuhan, and the taxi service operated without being influenced by the experiment.

2.2 Data collection and preprocessing

Although a large volume of data and parameters have been collected during the experiment, this study focuses on analyzing nine of these parameters. To comprehensively represent driving behavior, the information of pedal state, speed, and acceleration are used. In addition, ambient temperature is considered in this study to account for its significant impact on the operating range of battery voltage[47]. These parameters were collected at sampling frequencies between 1 Hz to 100 Hz, which is significantly higher than the data collected in previous works. The 249-day data from one experiment vehicle is extracted and preprocessed for the study. Firstly, the outliers are screened using the normal ranges of these parameters, and the missing values are identified. Then, the null values and outliers are replaced using nearest neighbor interpolation. Secondly, resampling is conducted to achieve the time alignment of these parameters, leading to the frequency of 1 Hz for all parameters after processing. After the data preprocessing, a total of 6163447 samples are obtained eventually. The extracted nine parameters and their statistics for 249-day operation data after preprocessing are shown in Table 2.

Table 2 Nine extracted parameters and their statistics for 249-day operation data

Data type	Unit	Original frequency	Mean	SD	Minimum	Maximum
Accelerator pedal stroke	%	10 Hz	8.69	13.26	0.00	99.00
Brake pedal stroke	%	10 Hz	0.77	1.92	0.00	42.00
Speed	km/h	100 Hz	20.94	23.94	0.00	125.45
Acceleration	m/s^2	10 Hz	0.49 (accelerate) / -0.49 (decelerate)	0.51	-6.52	4.95
Ambient temperature	℃	10 Hz	24.60	10.23	0.00	48.00
Pack voltage	V	50 Hz	373.12	13.85	332.00	401.00
Cell voltage	V	1 Hz	—	—	—	—
Current	A	50 Hz	-31.03 (charge) / 21.04 (discharge)	33.37	-164.00	251.00

SOC	%	50 Hz	75.32		14.74	23.80	99.30

3. Methodology

3.1 Segments identification and DBPs extraction

During the running of EVs, the driver's behavior of pressing/releasing pedal causes the battery to switch between two main modes: discharging and charging. The differences in these working modes may impact the VCC. Obviously, more accurate and reliable results would be obtained if analyzing the association between driving behavior and VCC for the battery under different working modes. Therefore, based on the driver's behavior in pressing/releasing pedal, we divide the running process of EVs into different types of segments, during which the working state and signal fluctuation mechanism of the battery vary. To elucidate the fluctuation mechanisms of battery signals along with driving behavior and the division method in driving segments, the curves of relevant parameters during a short period of operation on January 28, 2022, from one experimental vehicle are depicted in Fig. 3.

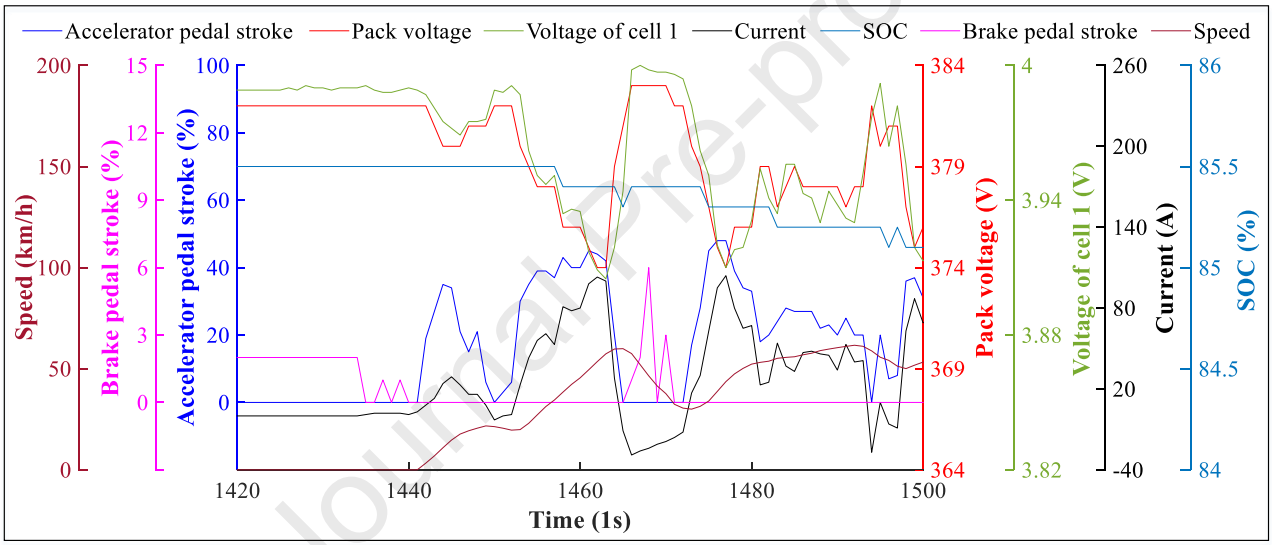

Fig. 3 Driving behavior profiles and battery signals during a short period of operation

As shown in Fig. 3, the curves of accelerator pedal stroke and current exhibit similar trends, while the voltage and current curves indicate opposite trends by roughly displaying a symmetric distribution. As accelerator pedal stroke increases, the current correspondingly rises and the battery voltage decreases. Conversely, when the brake pedal gets pressed, the current decreases and then transforms to be negative, while the voltage increases. According to the working mechanism of the battery during EVs operation, pressing accelerator pedal implies the battery energy output. On the other hand, when the brake pedal is pressed, regenerative braking is combined with traditional mechanical braking to decelerate the vehicle, and battery energy recovery is triggered. Therefore, the variation mechanisms of voltage are different in these two conditions. Additionally, under the condition of vehicle sliding with foot unused after releasing accelerator pedal completely, the positive current decreases and transitions to be negative, as shown around 1465 s in Fig. 3. It should be noted that this is a general varying mode. When the accelerator pedal is released rapidly, the current is negative before the pedal gets fully released. Conversely, under the condition of foot unused after releasing brake pedal completely, the negative current decreases and transitions to be positive, as shown around 1440 s and 1472 s in Fig. 3. Hence, among the different driving conditions, the fluctuation patterns of current and voltage are different. After this analysis, we opted for dividing EVs' running process into four types of segments based on driver's driving behavior of pressing/releasing pedals, i.e., segments A with driver's foot on

accelerator pedal, segments B with foot idle after completely releasing accelerator pedal, segments C with driver's foot on brake pedal, segments D with foot idle after completely releasing brake pedal. The schematic of the proposed segments dividing method is shown in Fig. 4. It should be noted that the segments when the vehicle is stopped are removed in this study.

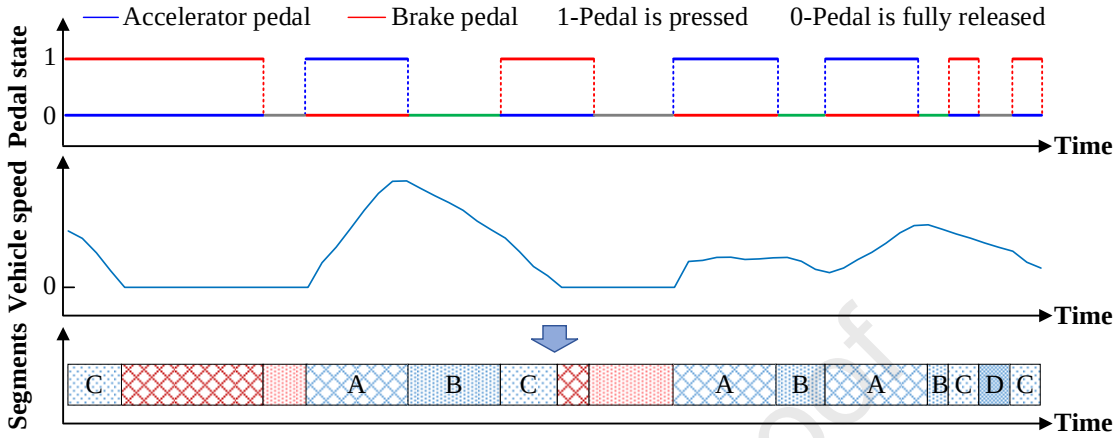

Fig. 4 Schematic of running segment division based on pedal status

Furthermore, operational data with a duration of 60 seconds was extracted as a visualization example to illustrate the results of segment division. As shown in Fig. 5, The range and SD of cell voltages fluctuate in real-time with the driving behavior state. The voltage range and SD curves exhibit similar trends to that of accelerator pedal stroke, a larger accelerator pedal stroke generally leads to a larger range and SD of cell voltages. Similarly, a larger brake pedal stroke tends to correspond to more significant voltage inconsistency, as the performance differences between cells are more pronounced during high discharging or charging current. Furthermore, segments A demonstrate the most significant voltage fluctuation and voltage inconsistency among the four segments overall. These results indicate that, driving behavior has a remarkable impact on the voltage consistency state and separate modeling as well as analysis for each segment are necessary.

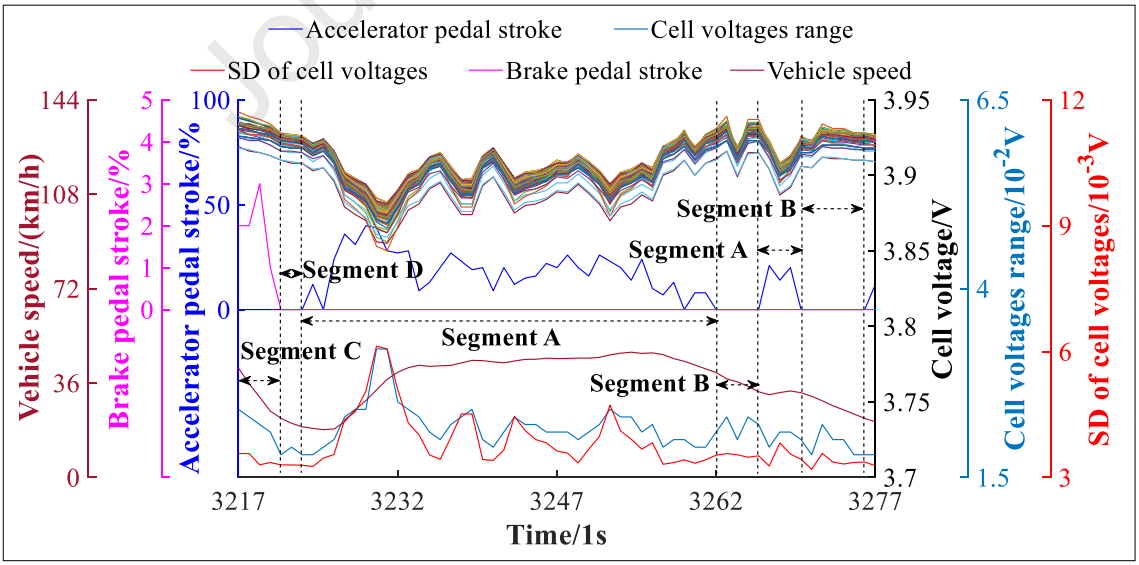

Fig. 5. Segment division visualization for the running process in a time window of 60 seconds

There are segments with very short durations during the running of the studied vehicle, which are not long enough to provide meaningful results. Therefore, samples with a duration of less than 5 s are excluded for segments B, C, D, and 10 s for segments A; these durations are deemed a good compromise between the accuracy of the

results and the complexity associated to the subsequent analysis and regression models discussed in the following sections. Indeed, while it is deemed out of scope for the present work, a rigorous analysis of the optimal value of the minimum segment duration would be needed for a real-time voltage inconsistency detection algorithm.

After processing, the number of segments A, B, C, and D is 76034, 18154, 20433, and 8050, respectively. Then, the DBPs (reported in Table 3) are extracted for each segment to describe driving behavior characteristics in terms of vehicle speed, acceleration, and pedal state.

Table 3 Description of the extracted DBPs for segments A, B, C, and D

Segments	No.	DBPs	Unit
A/B/C/D	1	Maximum speed	km/h
	2	Average speed	km/h
	3	SD of speed	km/h
	4	Maximum positive acceleration	m/s^2
	5	Maximum negative acceleration	m/s^2
	6	SD of acceleration	m/s^2
	7	Average positive acceleration	m/s^2
	8	Average negative acceleration	m/s^2
A	9	Maximum accelerator pedal stroke	%
	10	Average accelerator pedal stroke	%
	11	SD of accelerator pedal stroke	%
C	9	Maximum brake pedal stroke	%
	10	Average brake pedal stroke	%
	11	SD of brake pedal stroke	%

3.2 Quantitative characterization of VCC

The variation coefficient can describe the overall fluctuation characteristics of data over a time interval. Compared to other indicators such as entropy, distance between curves, variation coefficient is easier to calculate and requires less computational efforts in practice. Hence, following the works of [37][49], we adopted the VVCC to quantify voltage consistency during a segment. The calculation for VVCC can be expressed as:

$$\overline{V}_j = \frac{1}{n}\sum_{i=1}^{n} V_{ij}\ ,\ j = 1, 2, \ldots, k \tag{1}$$

$$\overline{V} = \frac{1}{k}\sum_{j=1}^{k} \overline{V}_j \tag{2}$$

$$V\max_j = \max\{V_{1j}, V_{2j}, \ldots, V_{nj}\}\ ,\ j = 1, 2, \ldots, k \tag{3}$$

$$V\min_j = \min\{V_{1j}, V_{2j}, \ldots, V_{nj}\}\ ,\ j = 1, 2, \ldots, k \tag{4}$$

$$\delta = \frac{\sqrt{\frac{1}{k}\sum_{j=1}^{k}(V\max_j - V\min_j)^2}}{\overline{V}} \tag{5}$$

where, V_{ij} represents the voltage value of the *i* cell at the sampling time *j*; the total number of cells is *n* (*n* is 96 in this paper); $\overline{V}_j$ represents the average voltage of all cells at the sampling time *j*; $\overline{V}$ is the average value of voltage during the segment; $V\max_j$ and $V\min_j$ represent the maximum and minimum of voltage at the sampling time *j*; δ is the VVCC during the segment. A larger value of VVCC means a worse VCC.

3.3 PCC based correlation analysis

According to the analysis carried out in section 3.1 for the curves of pedal, voltage, and current, there is a significant correlation between battery voltage and driving behavior. Therefore, the PCC is adopted to quantify the correlation between DBPs and the VVCC under four types of segments. For two random variables X and Y, the Pearson coefficient *R(X,Y)* can be calculated as follows:

$$R(X,Y)=\frac{Cov(X,Y)}{\sqrt{D(X)}\sqrt{D(Y)}}=\frac{\sum_{l=1}^{m}(x_l-\bar{x})(y_l-\bar{y})}{\sqrt{\sum_{l=1}^{m}(x_l-\bar{x})^2}\sqrt{\sum_{l=1}^{m}(y_l-\bar{y})^2}} \tag{6}$$

where *Cov*(*X*,*Y*) is the covariance between *X* and *Y*, $\sqrt{D(X)}$ and $\sqrt{D(Y)}$ are the standard deviations of *X* and *Y*, respectively, $\bar{x}$ and $\bar{y}$ are the means of *X* and *Y*, respectively, and *m* represents sample size.

The coefficient value is always within the interval [-1,1], and the larger its absolute value, the stronger the correlation between variables. Generally speaking, values of 0.8~1.0 are considered to indicate extremely strong correlation, whereas values of 0~0.2 suggest very weak correlation or no correlation[47].

3.4 RF regression models

In order to investigate the relationship between the DBPs and the VVCC, a regression model is developed. Because the features (i.e., the DBPs) to be used in this study have significant intercorrelation, all regression models that require non-correlation between features were discarded. A RF model[50] is selected because it has no requirement of non-correlation between features, allowing us to use all features as inputs to the model. Moreover, in contrast to other *black-box* artificial intelligence models, RF model has a strong interpretability thanks to that the contribution of features to target prediction can be directly obtained. Besides, combined with marginal impacts calculation method, RF models can effectively examine the relationships between features and the target. To achieve robust results over the different driving scenarios, one RF regression model is established for each kind of driving segments (one for segments A, one for segments B, etc.) to analyze the DBPs' importance and influence mechanism to VCC. In addition to the DBPs, the ambient temperature and SOC were also used as input features for the model, while the target variable is VVCC.

After training a RF model, the importance score of each feature is outputted. The score represents a feature's contribution degree to target regression and prediction, and it is quantified by the percentage increase in mean squared error (IncMSE%) of the out-of-bag data. In short, IncMSE% of a feature indicates the prediction accuracy decrease after that feature is removed, so a more important variable has a higher IncMSE%.

3.5 Analysis and interpretation of the RF models

After training the RF regression models, we assess how the driver behavior parameters affect VVCC, and whether their relationships are nonlinear, monotonic, or more complex. In order to interpret *black-box* machine learning models such as RF and ANN, partial dependence plot (PDP)[51] or accumulated local effect (ALE)[52] plots are typically used. Both these tools graphically describe the impact of each feature on the response variable. More specifically, they display the average marginal effect of each feature on the prediction. However, PDP assumes that the features are completely independent from each other. Therefore, given the expected inter-dependence of the DBPs, PDP is unsuitable for our model. On the other hand, ALE was specifically developed to handle intercorrelated features. Hence, this method was selected in this work to investigate the marginal effect of each individual DBP on voltage inconsistency, i.e., how the effect of an individual DBP changes the VVCC when other parameters are held constant.

The underlying idea behind ALE can be summarized as follows. Suppose that $\hat{f}(\cdot)$ is a regression model. For a feature x_e, the local effect of x_e on the response variable can be expressed by the partial derivative $\hat{f}^e(\cdot)$:

$$\hat{f}^e(x_e,x_c)=\partial\hat{f}(x_e,x_c)/\partial x_e \tag{7}$$

The variables x_c refer to all the other features of the model, excluding x_e. Then, the value of ALE for feature x_e at a

given value of $x_e = x$ is the accumulated value of this partial derivative (or rather its expected value) from $x_e = 0$ to x.

In practice, regression models based on machine-learning are not differentiable and the partial derivative in Eq. (7) must be approximated. This is done by dividing the feature space for x_e into a finite number of intervals and replacing the values of x_e with gridded values (the intervals' bounds). The partial derivative in Eq. (7) is approximated, for each interval I_k, by the difference: $\hat{f}(z_{(k)}, x_c) - \hat{f}(z_{(k-1)}, x_c)$, where $z_{(k-1)}$ and $z_{(k)}$ are the left and right bounds of I_k; this difference is evaluated for all data points for which the value of x_e lies in I_k. The value of the ALE can then be obtained by accumulating these differences. The specific calculation steps were provided in the work of Apley et al.[52].

4.Results and discussions

4.1 Correlation between DBPs and VVCC

The PCCs between VVCC and DBPs are illustrated in Fig. 6. As shown in Fig. 6, for segments A, the two parameters most correlated with VVCC are average accelerator pedal stroke and maximum accelerator pedal stroke. The explanation for this high correlation is that the driver's engagement with accelerator pedal directly influences voltage fluctuations so that their curves are roughly symmetrical. Additionally, maximum speed, SD of accelerator pedal stroke, average positive acceleration and SD of speed show a moderate correlation with VVCC. The two parameters having the lowest correlation are average negative acceleration and maximum negative acceleration, since EVs operate primarily by driving and energy output modes during segments A without involving instances of large deceleration. In situations requiring rapid deceleration, the driver tends to release the accelerator pedal completely and engage brake pedal. For segments C, the two parameters most correlated with VVCC are average speed and maximum speed, which both show a moderate correlation. This can be explained by the fact that the intensity of regenerative braking is directly influenced by vehicle speed. Generally speaking, the higher the vehicle speed, the greater the energy recovery intensity, and therefore, at a higher speed, a larger regenerative braking torque can be generated. In other words, energy recovery essentially involves converting kinetic energy into electrical energy. Therefore, the vehicle at higher speed would make a greater intensity of energy recovery due to its carried larger kinetic energy. Therefore, average speed, maximum speed, and SD of speed exhibit the most prominent correlation with VVCC under these segments. The three brake-pedal-stroke related parameters are weakly correlated with VVCC. During segments C, regenerative braking and traditional mechanical braking usually work together to decelerate the vehicle. The braking force allocation between regenerative braking and mechanical braking involves a complicated strategy set by vehicle manufacturer. Since the battery energy recovery is solely related to regenerative braking and independent of mechanical braking, the relationship between brake pedal stroke and battery charging current is nonlinear. Hence, the correlation with VVCC of brake-pedal-stroke related parameters are weaker than speed related parameters.

In segments B and D, the vehicle is on coasting and the energy recovery made by regenerative braking is the primary factor influencing voltage fluctuation. As mentioned before, the intensity of regenerative braking largely depends on coasting speed, a higher speed generally leads to a more violent regenerative braking. Therefore, under these two segments, the three parameters most correlated with VVCC are also average speed, maximum speed, and SD of speed. Additionally, it is observed that the PCC values of these three parameters in segments D are lower than that in segments B. As the subsequent segments to braking segments C, segments D often have more lower speed than segments B, resulting in smaller energy recovery intensity and voltage fluctuation.

For segments B, C, and D, despite some differences on vehicle operation and battery mode transitions, the

battery is essentially in a charging state through energy recovery. Hence, the correlation results for the three types of segments are quite similar, with the same four most correlated parameters and same four parameters holding weakest correlation. Moreover, for segments B, C, and D, the correlations of acceleration related parameters with VVCC are weaker than that of speed related parameters.

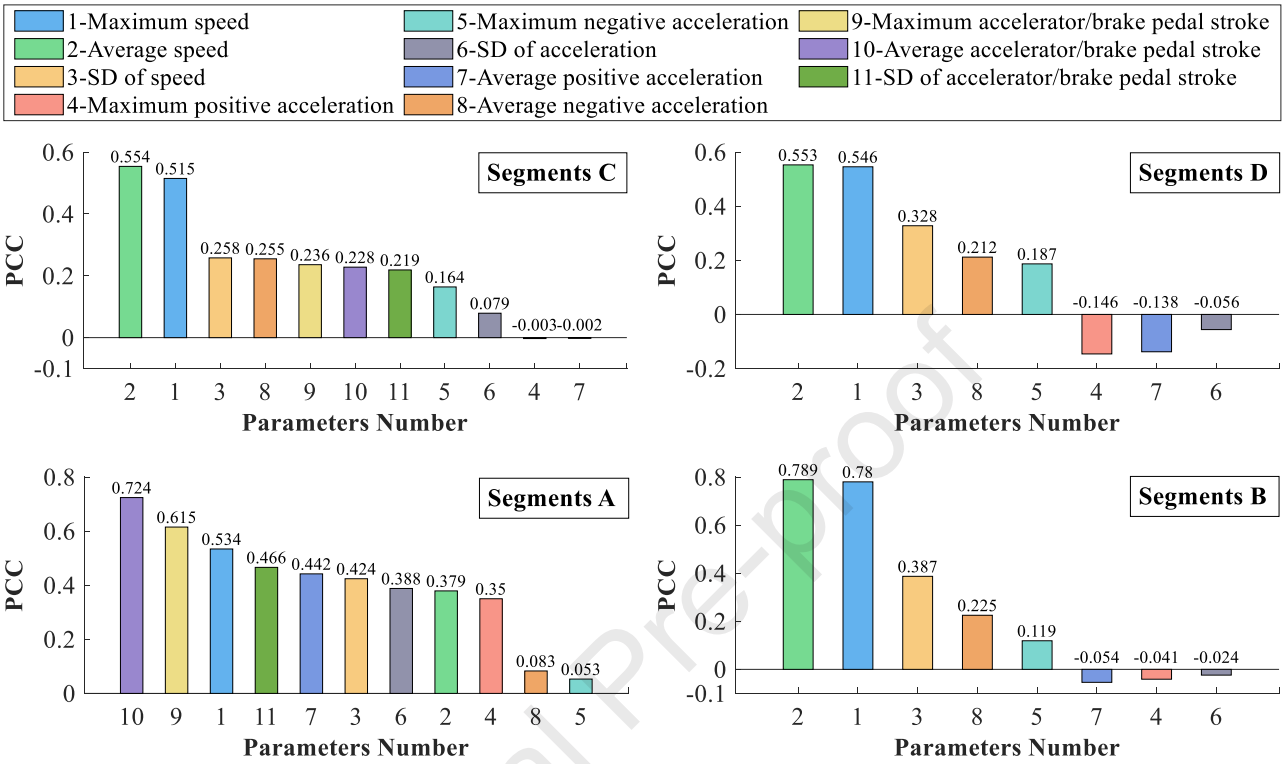

Fig. 6 PCCs between VVCC and DBPs

4.2 Impact mode of DBPs on VVCC

As part of the training process for the four RF models, some hyper-parameters, such as number of decision trees, maximum depth of trees, and maximum number of features, are optimized. First, the number of decision trees for all four RF models is determined through the 3-fold cross-validation method, and eventually, 200 is set for each model as a good compromise between the training time and accuracy of the results. Then, the optimal values of the other hyper-parameters are determined using grid search and 3-fold cross-validation. The obtained optimal hyper-parameter values and goodness of fit which is quantified by the coefficient of determination R^2, after model training are presented in Table 4. The value of R^2 for the RF models of segments A, B, C, and D is 0.919, 0.946, 0.955, and 0.955, respectively. These values suggest that all RF models have good prediction accuracy. The results of feature importance are quantified through IncMSE%, as illustrated in Fig. 7. It is noteworthy that the SOC and ambient temperature were selected along with DBPs as inputs due to their significant impacts on voltage, in order to establish RF models with a high accuracy. Therefore, in Fig. 7, the results of SOC and ambient temperature are also illustrated. As Fig. 7 shows, it is observed that SOC is consistently significant for all four types of segments, especially in segments C and D, while the importance of ambient temperature is not pronounced. Indeed, as SOC goes down, battery voltage gradually decreases. Thus, battery SOC influences the fluctuation range of voltage, establishing a close connection with VVCC.

Table 4 Optimal hyper-parameter values and goodness of fit of developed RF models

Segments	Hyper-parameters					R^2
	Number of trees	Maximum depth of trees	Minimum number of samples to split an internal node	Minimum number of samples in a leaf	Maximum number of features	
A	200	25	3	1	0.7	0.919
B	200	15	5	2	0.7	0.946
C	200	16	2	1	0.5	0.955
D	200	25	4	1	0.5	0.955

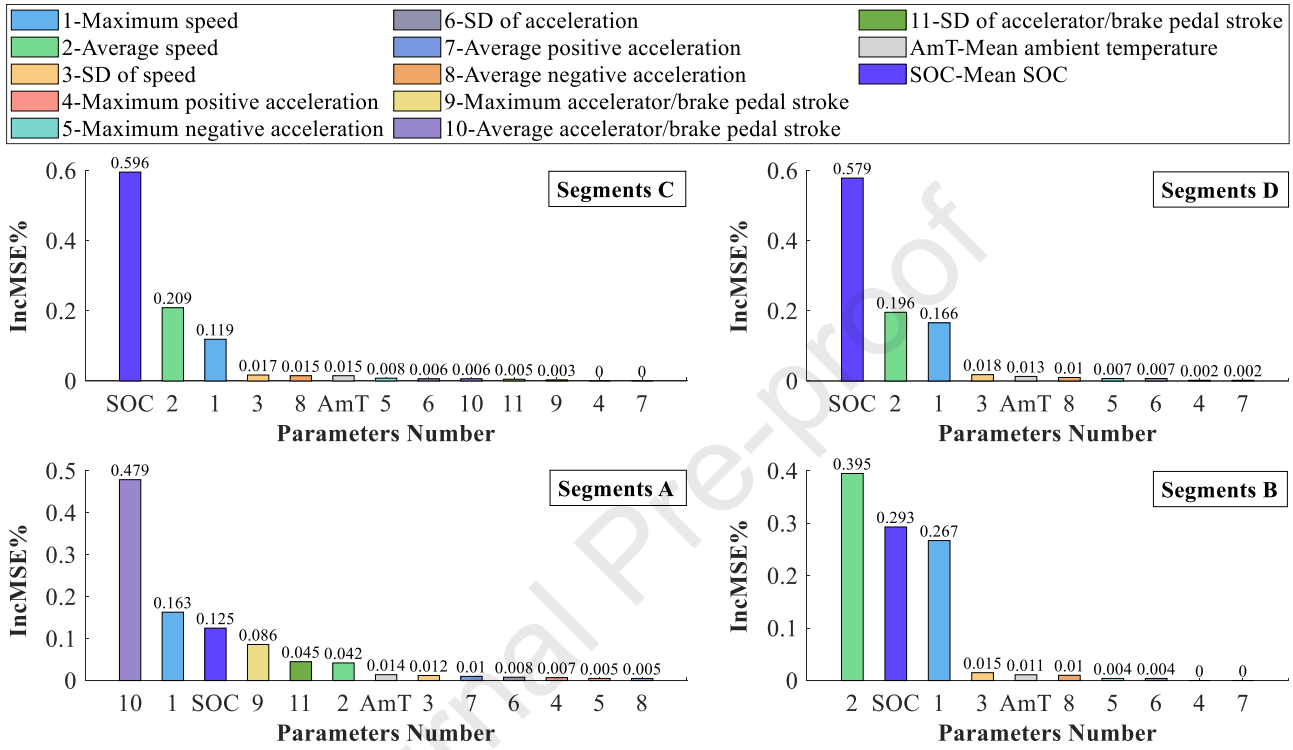

Fig. 7 Importance of features to VVCC regression and prediction

Regarding the DBPs, it can be seen from Fig. 6 and Fig. 7 that the four most important DBPs for each segment type are the same, whether Pearson's coefficient or the IncMSE is considered as a metric. Therefore, these parameters were selected for further exploring their impact patterns on voltage inconsistency.

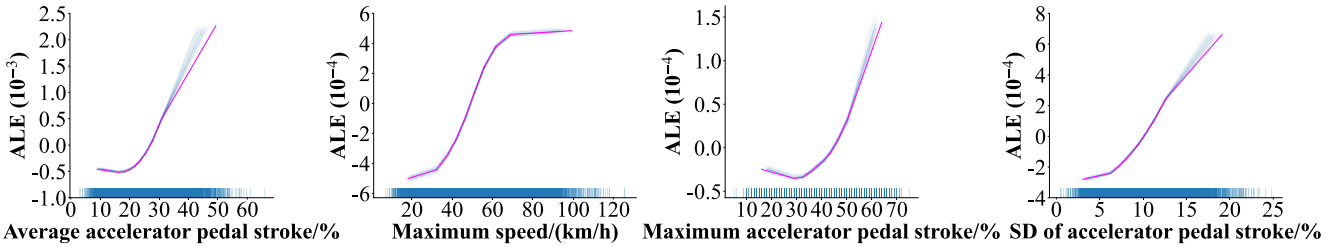

(a) Segments A

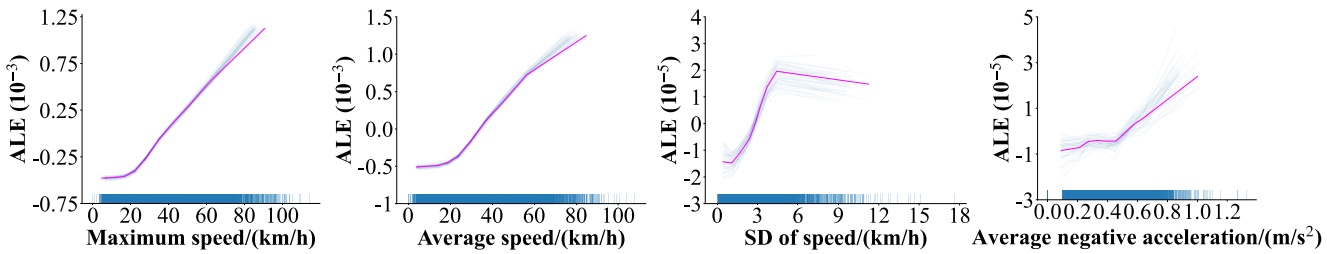

(b) Segments B

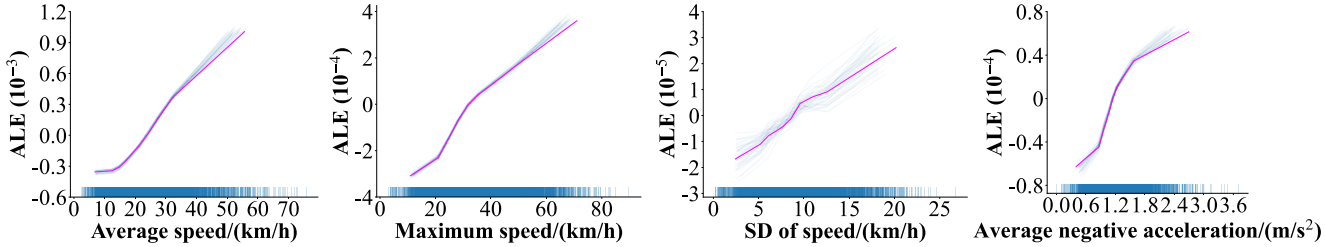

(c) Segments C

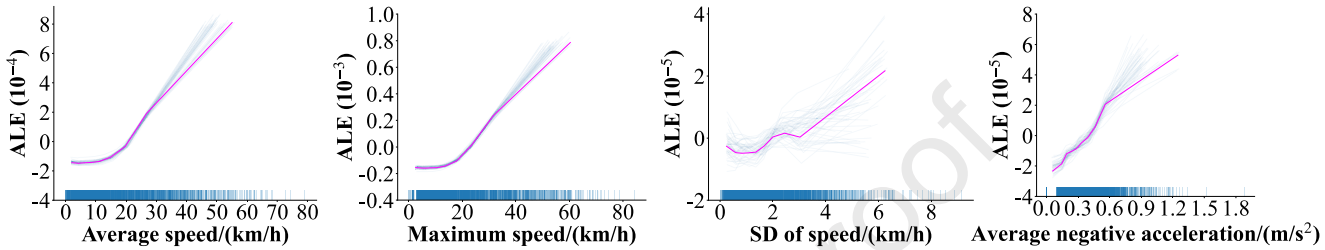

(d) Segments D

Fig. 8 ALE of important DBPs on VVCC

Fig. 8 illustrates the ALE of these important DBPs on VVCC. The magenta curve represents the ALE based on all training data, while the light blue curves for reference are derived from 50 bootstrap experiments where one-tenth of the training data is sampled. These light blue curves show the differences between multiple experimental results: the closer the distances between these curves, the clearer the relationship between the feature and dependent variable. It can be seen from Fig. 8 (a), under segments A, as average accelerator pedal stroke increases, ALE shows a slight decrease before rapidly increasing, the transition point from decrease to increase occurs at approximately 17%. It should be noted that the increase of ALE means the rising of VVCC and the deterioration of voltage consistency. For maximum speed, the ALE monotonically increases, with high rate within the range of 33-68 km/h but very low rate when beyond 68 km/h. For vehicles running on urban road, maximum speed may keep rising after exceeding 68 km/h, but average speed and average pedal stroke would not increase consistently. Average accelerator pedal stroke is the most crucial parameter affecting VVCC, hence, the change of ALE is minimal after maximum speed exceeds 68 km/h. For maximum accelerator pedal stroke, the ALE continuously decreases when it below 29%, then steadily increases after it exceeds 29%, so the influence pattern is similar to that of average accelerator pedal stroke. Additionally, ALE increases monotonically with SD of accelerator pedal stroke.

Under segments B, C, and D, the ALE curves of average speed and maximum speed show a tendency of continuous rising, and exhibit an approximate linear upward trend when over a certain speed threshold. This trend is attributed to the strong correlation between vehicle speed and voltage fluctuation during energy recovery. Additionally, the ALE of average negative acceleration in all three types of segments almost consistently increases, mirroring the pattern observed in average speed. A higher average deceleration is often translated into a greater conversion of kinetic energy into electrical energy and more pronounced voltage fluctuations, although the average deceleration is weakly correlated with VVCC. However, for SD of speed under segments B, the ALE primarily increases before slowly decreasing, which shows a notable difference from segments C and D.

Overall, these important DBPs exhibit a positive influence on the increase of VVCC. Their relationships with VVCC are nonlinear, yet approximate a linear association within certain ranges, particularly for average accelerator pedal stroke, SD of accelerator pedal stroke, average speed, and maximum speed. The non-linear relationships contribute to a better understanding of the driving behavior's impact pattern on VVCC.

4.3 Actual effects of DBPs on VVCC

The ALE can only describe the theoretical non-linear relationships between DBPs and VVCC, failing to express the actual magnitude of their impact on VVCC. Therefore, the authors further conduct a quantitative and more intuitive analysis of their actual effects based on data statistics. The segment samples are divided into four groups for each DBP, based on their quantiles of 25%, 50%, and 75%. Subsequently, the growth rate on mean VVCC for the latter three groups (quantile 25%-50%, 50%-75%, and 75%-100%) with respect to the first group (below quantile 25%) is used to characterize the magnitude of the effects of the DBP on voltage consistency.

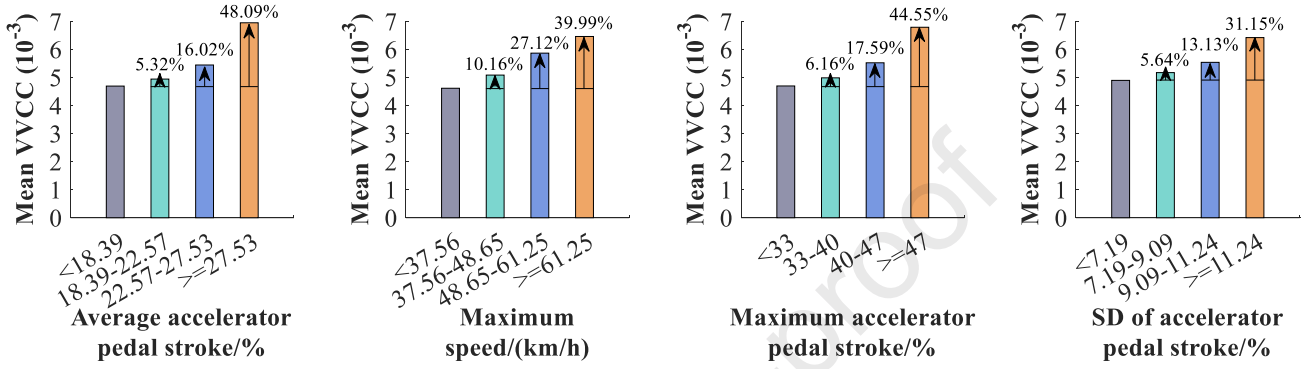

(a) Segments A

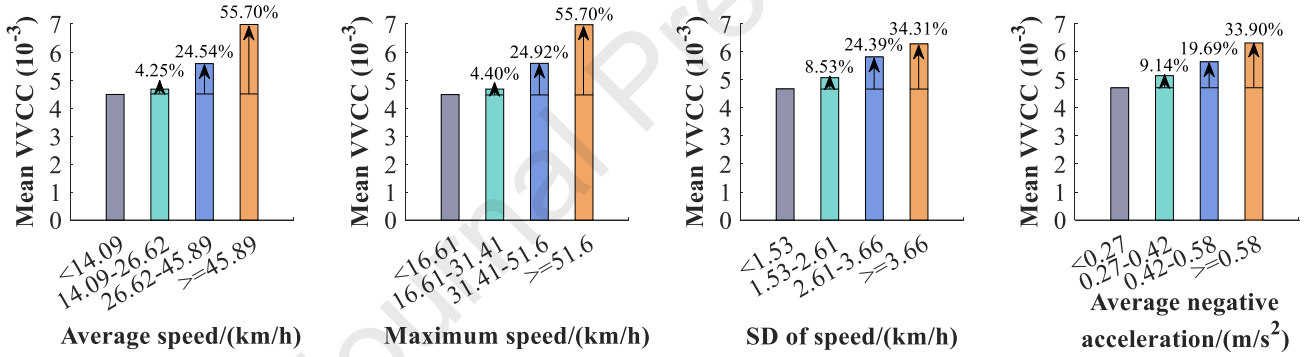

(b) Segments B

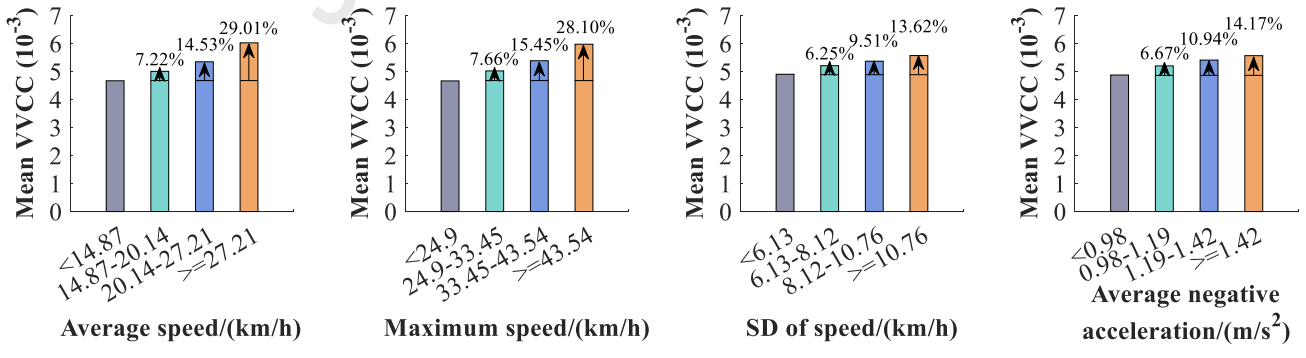

(c) Segments C

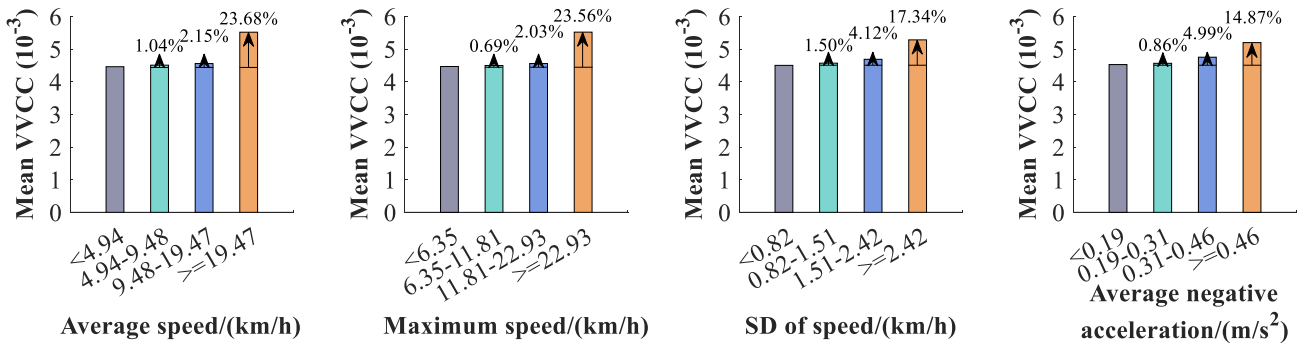

(d) Segments D

Fig. 9 DBPs' actual effects quantified by growth rate of mean VVCC

As shown in Fig. 9, for all the involved parameters, groups with higher DBP value have larger mean value of VVCC, which further indicates that an increase in these parameter values leads to a deterioration in VCC. Indeed, in Fig. 9 (a), the maximum growing rates of mean VVCC are obtained by DBP values above 75th percentile at segments A. From this perspective, the most significant effect is observed on average accelerator pedal stroke. However, within the range of quantile 50%-75%, the most significant effect is observed on maximum speed which reaches 27.12%. As seen from Fig. 9 (b), (c), and (d), for segments B, C, and D, the effects of average speed and maximum speed on VVCC are very similar. For these two DBPs, the effect is the most significant over segments B, while is the lowest under segments D due to their lowest speed, minimal battery charging current and voltage fluctuation overall. Under segments B, the maximum effects of SD of speed and average negative acceleration are 34.31% and 33.90%, respectively, while their values are below 18% under segments C and D. Additionally, by comparison overall, segments D exhibits the lowest effect of DBPs on VVCC, followed by segments C. For segments B, the maximum effects of average speed and maximum speed both reach 55.70%, making them the largest among all DBPs under the four kinds of segments.

To more directly reflect the effects of driving behavior on VVCC across the four categories of segments, the maximum quantified effects of these DBPs are summarized in Table 5. Segments B exhibits the most significant effects of DBPs on VVCC, while segments D show the weakest effects. For segments B, the maximum effects of average speed and maximum speed both reach 55.70%, while that of average accelerator pedal stroke under segments A is 48.09%. Compared to segments A, the overall speed is lower and the speed interval is larger in segments B. Therefore, the difference in VVCC between high-speed (above quantile 75%) and low-speed (below quantile 25%) states is more pronounced in segments B. Additionally, the weak effects of driving behavior on VVCC under segments D are attributed to the relatively small differences in speed within the segment.

Table 5 Maximum quantitative effects of important DBPs on VVCC

DBPs	Effects (%)	DBPs	Effects (%)		
	Segments A		Segments B	Segments C	Segments D
Average accelerator pedal stroke	48.09	Average speed	55.70	29.01	23.68
Maximum speed	39.99	Maximum speed	55.70	28.10	23.56
Maximum accelerator pedal stroke	44.55	SD of speed	34.31	13.62	17.34
SD of accelerator pedal stroke	31.15	Average negative acceleration	33.90	14.17	14.87

It is important to note that DBPs under segments B generally exhibit the most significant effects measured by the growing rate, but this does not necessarily mean the VVCC is highest in these segments. We calculated the average VVCC for each kind of segments under different ambient temperatures and SOC conditions, as shown in Fig. 10. The ambient temperature range of the dataset is from 0 ℃ to 48 ℃, and the SOC range is from 23.8% to 99.3%. We group the segments by the interval of 8 ℃ for ambient temperature and 20% for SOC, which can achieve that as much groups as possible are obtained and the situation of dividing scanty samples in certain groups is avoided. From Fig. 10, it is evident that SOC also has a significant impact on VVCC. Under SOC conditions ranging from 20% to

60%, segments A exhibits the highest mean VVCC for almost all ambient temperatures, followed by segments B and then segments C. This is primarily because, as mentioned earlier, segments A has the highest speed and the most drastic current changes overall, while segment D has the lowest. However, under SOC conditions ranging from 60% to 100%, the differences in mean VVCC among the four kinds of segments are obviously reducing, and segments A does not always exhibit the highest average VVCC, nor does segment D show the lowest. These results demonstrate that SOC, ambient temperature, and driving behavior collectively influence voltage consistency. Therefore, the established thresholds need adapt not only to driving behavior but also to environmental factors and the battery's own state.

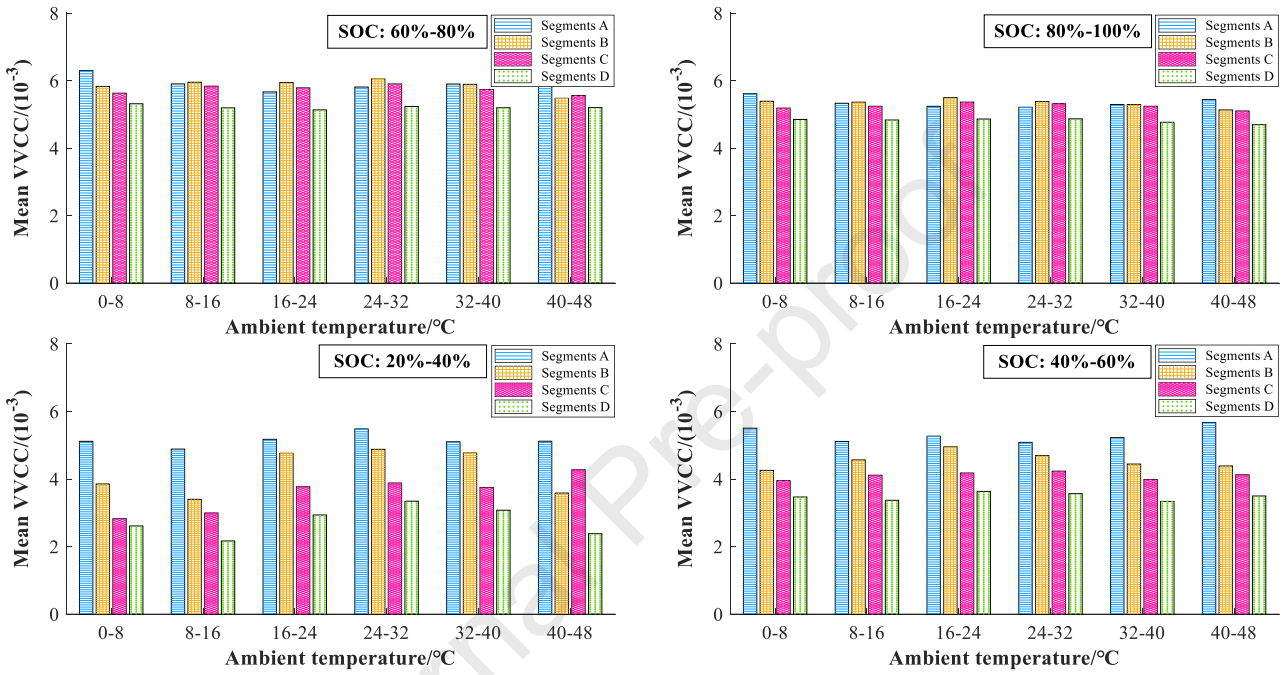

Fig. 10 Comparison of mean VVCC among four kinds of segments under different ambient temperature and SOC conditions

The above results intuitively demonstrate and quantify the impact of the DBPs on VVCC. They also directly emphasize the necessity of integrating driving behavior for evaluating and diagnosing voltage inconsistency. Based on these findings, it is evident that integrating parameters of average accelerator pedal stroke, maximum speed, and maximum accelerator pedal stroke at segments A, along with average speed and maximum speed at segments B, is crucial for voltage inconsistency evaluation and diagnosis. This integration can maximize the accuracy of VCC evaluation and diagnosis. Clearly, for detecting abnormal VVCC using a threshold-based method, larger thresholds should be applied to running states with higher VVCC. For instance, a rough estimation suggests that, for segments A with average accelerator pedal stroke exceeding 27.53%, the threshold should be approximately 1.48 times larger than that of segments below 18.39%, since the mean VVCC corresponding to the average accelerator pedal stroke above 75th percentile is 48.09% higher than that below 25th percentile. In summary, these results not only contribute to understanding the extent of driving behavior's impact on VVCC, but also provide insights for setting thresholds in engineering practices for voltage inconsistency evaluation and diagnosis.

4.4 Implications for voltage inconsistency detection

Based on the results presented above, it is evident that voltage inconsistency exhibits a high sensitivity to driving behavior. Thus, as previously mentioned, both single fixed threshold and multiple fixed thresholds for different operating scenarios have limitations in detecting voltage inconsistency, and a robust fault detection method should use adaptive rather than fixed thresholds. Setting adaptive thresholds, also known as real-time dynamic

thresholds, relies on utilizing the real-time mapping relationship between VCC and driving behavior. The results of this study show a possibility for the application of such methods. Meanwhile, the breakthroughs of artificial intelligence algorithms and the development of platforms using high-frequency data provide a solid foundation for the application. Currently, due to the rapid development of EVs worldwide, there is a growing trend globally towards utilizing high-frequency operational data for battery and vehicle safety monitoring and control. In addition, to meet personalized safety monitoring requirements from automobile manufacturers and automotive service providers, there is already a telematics-box available in the market with the data collection and upload frequency of 1 Hz. Meanwhile, it is designed with sufficient model computing and analysis capability, which enables comprehensive data collection and computation for on-board safety monitoring and warning. On the other hand, with the rapid development of artificial intelligence and the explosive growth of vehicular operation data, powerful deep learning algorithms such as LSTM, convolutional neural network (CNN), and TCN would be increasingly applied to battery state prediction as well as risk warnings with considering vehicle running conditions. Therefore, the findings of this study have broad application prospects in future upgraded EVs management platforms for voltage inconsistency detection.

The findings of this study can effectively support the development of adaptive threshold-based method. Firstly, based on the results of PCC and parameters importance, the most significant DBPs that should be preferentially selected as model inputs for prediction of VCC are identified. Secondly, this study reveals the impact patterns and actual effects of driving behavior on VCC, enhancing the model interpretability for interval prediction. This higher interpretability helps developers better understand the model and fosters user trust in the model results. Due to the "black box" nature of machine learning models, especially ANN, their interpretability becomes more and more important along with their increasing application in battery state prediction. According to the high accuracy showed by the RF models in this work, it is found that accurate prediction of VCC can be achieved, and interval prediction based on machine learning algorithms is well-suited for voltage inconsistency detection. The suggested method is illustrated in Fig. 11. By using extensive operational data from normal vehicles and the extracted ambient temperature, SOC, and driving behavior parameters as features, models such as quantile regression forest and quantile regression neural network can predict the normal range of VCC during real-time vehicle operation. Once the real value of VCC exceeds the upper or lower limits of the normal interval at a certain confidence level, primarily the upper limit, abnormal values of VCC can be detected. In this framework, the predicted normal range would serve as an adaptive threshold, which changes along with vehicle's operation.

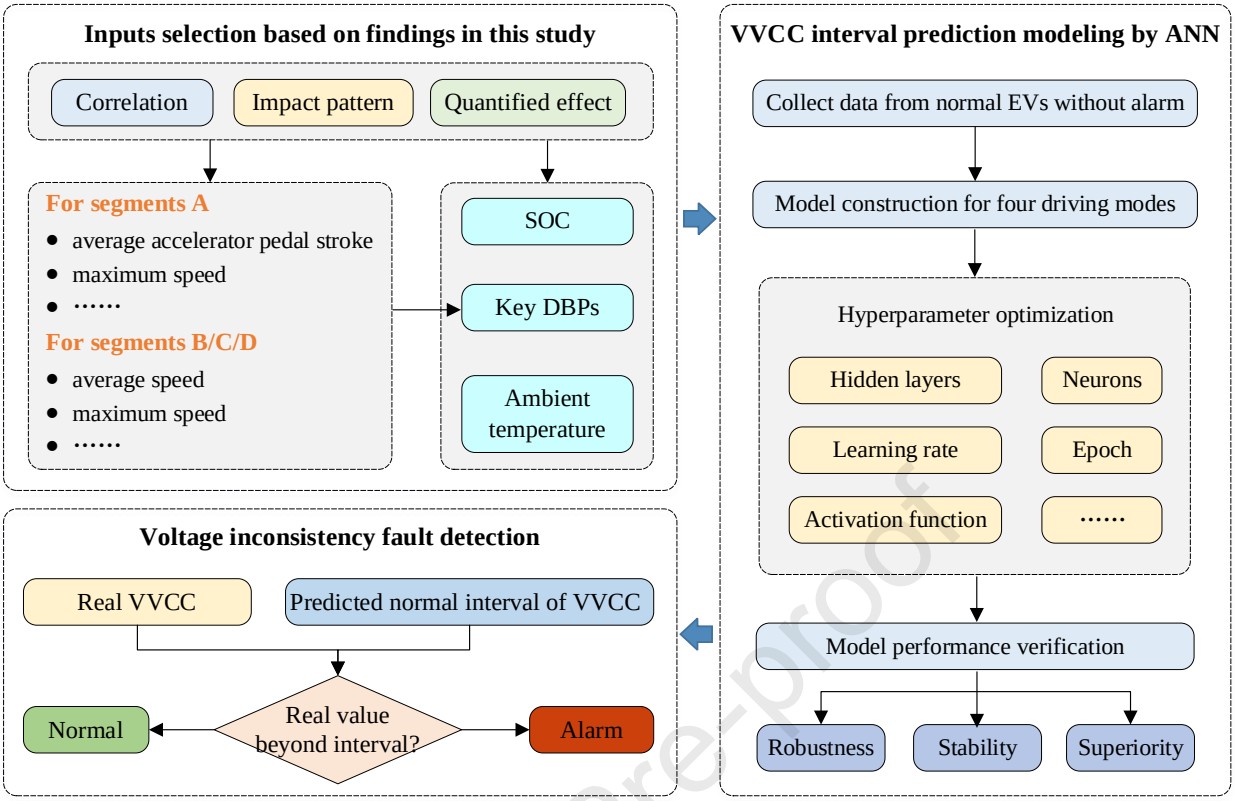

Fig. 11 Schematic of adaptive-threshold-based voltage inconsistency detection

5. Conclusions

Accurate evaluation and diagnosis of voltage inconsistency are crucial for ensuring the safety of battery system in EVs. This study explores the associations between driving behavior and voltage inconsistency, thus setting the basis for the development of an adaptive-threshold-based method to detect voltage inconsistency faults using the data from real-world EVs. After identifying different kinds of running segments of EVs, the correlation, impact patterns, and actual effects of driving behavior with respect to voltage consistency are analyzed for each segment type.

The key findings can be summarized as follows. First, a significant correlation between driving behavior and VVCC is observed over the experimental data. Specifically, the parameter most correlated with VVCC at segments A is average accelerator pedal stroke, with a PCC value of 0.724, while for segments B, C, and D, it is average speed, with PCC values of 0.789, 0.554, and 0.553, respectively. Secondly, the four RF models all show a high accuracy of VVCC prediction with R^2 over 0.919, which indicates that the relationships between VVCC and important DBPs can be effectively captured. Moreover, the ALE results demonstrate their relationships are positive-nonlinear overall, while approximately linear for most intervals. Thirdly, the data statistics verifies that the important DBPs have obvious promoting effects on VVCC for all kinds of running segments. The DBP with the maximum effect is average accelerator pedal stroke for segments A, and average speed for segments B, C, and D. The mean VVCC corresponding to their value above 75th percentile is respectively 48.09%, 55.70%, 29.01%, and 23.68% greater than that below 25th percentile. Hence, based on all the results, we can conclude that there is a strong connection between driving behavior and battery voltage consistency and there is the potential to use the proposed approach for predicting voltage consistency. Additionally, key parameters for modeling voltage inconsistency are identified, including average accelerator pedal stroke, maximum speed, maximum accelerator pedal stroke, SD of accelerator pedal stroke for segment A, and average speed, maximum speed, SD of speed, and average negative acceleration for the other three segments.

The findings in this study, as indicated by the correlation analysis and parameter importance, would provide crucial inputs for VCC prediction modeling in future works. The revealed impact patterns and actual effects of driving behavior on VCC could be utilized for interpreting and improving VCC prediction models. However, it is worth to point out the limitations of this research. Firstly, this study exclusively investigates VCC during vehicle motion and does not analyze the scenario of vehicle in a stationary state. Secondly, this research focuses specifically on VVCC, and the results from other indicators characterizing VVCC might exhibit slight variations. In future work, it would be worthwhile to explore the relationships between driving behavior and different VCC indicators, such as entropy, curve distance, and so forth, then establish corresponding prediction models. Furthermore, the performances of several models can be compared to identify the optimal model for voltage inconsistency evaluation and diagnosis.

References

[1] Hu G, Huang P, Bai Z, Wang Q, Qi K. Comprehensively analysis the failure evolution and safety evaluation of automotive lithium ion battery. eTransportation 2021;10.

[2] Li S, Zhang C, Du J, Cong X, Zhang L, Jiang Y, et al. Fault diagnosis for lithium-ion batteries in electric vehicles based on signal decomposition and two-dimensional feature clustering. Green Energy Intell Transport 2022;1(1).

[3] Liu Q, Ma J, Zhao X, Zhang K, Meng D. Online diagnosis and prediction of power battery voltage comprehensive faults for electric vehicles based on multi-parameter characterization and improved K-means method. Energy 2023;283.

[4] Tang X, Zou C, Wik T, Yao K, Xia Y, Wang Y, et al. Run-to-run control for active balancing of lithium iron phosphate battery packs. IEEE Trans Power Electron 2020;35(2):1499-512.

[5] García A, Monsalve-Serrano J, Sari R L, Martínez-Boggio S. Thermal runaway evaluation and thermal performance enhancement of a lithium-ion battery coupling cooling system and battery sub-models. Appl Therm Eng 2022;202.

[6] Chen J, Zhou Z, Zhou Z, Wang X, Liaw B. Impact of battery cell imbalance on electric vehicle range. Green Energy Intell Transport 2022;1(3).

[7] Guo R, Lu L, Ouyang M, Feng X. Mechanism of the entire overdischarge process and overdischarge-induced internal short circuit in lithium-ion batteries. Sci Rep 2016;6:30248.

[8] Feng X, Zhang X, Xiang Y. An inconsistency assessment method for backup battery packs based on time-series clustering. J Energy Storage 2020;31.

[9] Yang N, Zhang X, Shang B, Li G. Unbalanced discharging and aging due to temperature differences among the cells in a lithium-ion battery pack with parallel combination. J Power Sources 2016;306:733-41.

[10] Liao L, Li H, Li H, Jiang J, Wu T. Research on equalization scheme of lithium-ion battery packs based on consistency control strategy. J Energy Storage 2023;73.

[11] Shen D, Bai M, Yang D, Hinds G, Wang L, Lyu C. Detection and quantitative diagnosis of micro-short-circuit faults in lithium-ion battery packs considering cell inconsistency. Green Energy Intell Transport 2023.

[12] Chen C, Xiong R, Yang R, Li H. A novel data-driven method for mining battery open-circuit voltage characterization. Green Energy Intell Transport 2022;1(1).

[13] Schuster S F, Brand M J, Berg P, Gleissenberger M, Jossen A. Lithium-ion cell-to-cell variation during battery electric vehicle operation. J Power Sources 2015;297:242-51.

[14] Tian J, Liu X, Chen C, Xiao G, Wang Y, Kang Y, et al. Feature fusion-based inconsistency evaluation for battery pack: improved Gaussian mixture model. IEEE Trans Intell Transp Syst 2022;24(1):446-58.

[15] Ouyang D, Chen M, Liu J, Wei R, Weng J, Wang J. Investigation of a commercial lithium-ion battery under overcharge/over-discharge failure conditions. RSC Adv 2018;8(58):33414-24.

[16] Wang D, Bao Y, Shi J. Online Lithium-ion battery internal resistance measurement application in state-of-charge estimation using the extended Kalman filter. Energies 2017;10(9).
[17] Hong J, Wang Z, Qu C, Zhou Y, Shan T, Zhang J, et al. Investigation on overcharge-caused thermal runaway of lithium-ion batteries in real-world electric vehicles. Appl Energy 2022;321.
[18] Fang W, Chen H, Zhou F. Fault diagnosis for cell voltage inconsistency of a battery pack in electric vehicles based on real-world driving data. Comput Electr Eng 2022;102:108095.
[19] Wang G, Jin S, Jiao J, Xie J. Voltage measurement-based recursive adaptive method for internal short circuit fault diagnosis in lithium-ion battery packs. Control Eng Pract 2024;145.
[20] Tian J, Wang Y, Liu C, Chen Z. Consistency evaluation and cluster analysis for lithium-ion battery pack in electric vehicles. Energy 2020;194:116944.
[21] Feng F, Hu X, Hu L, Hu F, Li Y, Zhang L. Propagation mechanisms and diagnosis of parameter inconsistency within Li-Ion battery packs. Renew Sustain Energy Rev 2019;112:102-13.
[22] Duan B, Li Z, Gu P, Zhou Z, Zhang C. Evaluation of battery inconsistency based on information entropy. J Energy Storage 2018;16:160-66.
[23] Li X, Yuan C, Li X, Wang Z. State of health estimation for Li-Ion battery using incremental capacity analysis and Gaussian process regression. Energy 2020;190:116467.
[24] Zhang X, Wang Y, Wu J, Chen Z. A novel method for lithium-ion battery state of energy and state of power estimation based on multi-time-scale filter. Appl Energy 2018;216:442-51.
[25] Li D, Zhang Z, Liu P, Wang Z. DBSCAN-based thermal runaway diagnosis of battery systems for electric vehicles. Energies 2019;12(15).
[26] Hong J, Zhang H, Xu X. Thermal fault prognosis of lithium-ion batteries in real-world electric vehicles using self-attention mechanism networks. Appl Therm Eng 2023;226:120304.
[27] Lu J, Xiong R, Tian J, Wang C, Sun F. Deep learning to predict battery voltage behavior after uncertain cycling-induced degradation. J Power Sources 2023;581.
[28] Liu Y, Li Q, Wang K. Revealing the degradation patterns of lithium-ion batteries from impedance spectroscopy using variational auto-encoders. Energy Storage Mater 2024;69.
[29] Zhang H, Gao J, Kang L, Zhang Y, Wang L, Wang K. State of health estimation of lithium-ion batteries based on modified flower pollination algorithm-temporal convolutional network. Energy 2023;283.
[30] Hu X, Zhang K, Liu K, Lin X, Dey S, Onori S. Advanced fault diagnosis for lithium-Ion battery systems: A review of fault mechanisms, fault features, and diagnosis procedures. IEEE Ind Electron M 2020;14(3):65-91.
[31] Hua Y, Zhou S, Cui H, Liu X, Zhang C, Xu X, et al. A comprehensive review on inconsistency and equalization technology of lithium-ion battery for electric vehicles. Int J Energ Res 2020;44(14):11059-87.
[32] Kang Y, Duan B, Zhou Z, Shang Y, Zhang C. A multi-fault diagnostic method based on an interleaved voltage measurement topology for series connected battery packs. J Power Sources 2019;417:132-44.
[33] Liu Q, Ma J, Zhao X, Zhang K, Xiangli K, Meng D, et al. Voltage fault diagnosis and misdiagnosis analysis of battery systems using the modified Shannon entropy in real-world electric vehicles. J Energy Storage 2023;73.
[34] Wang Q, Wang Z, Zhang L, Liu P, Zhang Z. A novel consistency evaluation method for series-connected battery systems based on real-world operation data. IEEE Trans Transport Electrific 2021;7(2):437-51.
[35] Qiu Y, Cao W, Peng P, Jiang F. A novel entropy-based fault diagnosis and inconsistency evaluation approach for lithium-ion battery energy storage systems. J Energy Storage 2021;41.
[36] Li X, Wang Z. A novel fault diagnosis method for lithium-Ion battery packs of electric vehicles. Measurement 2018;116:402-11.
[37] Lu Y, Li K, Han X, Feng X, Chu Z, Lu L, et al. A method of cell-to-cell variation evaluation for battery packs in electric vehicles with charging cloud data. eTransportation 2020;6:100077.

[38] Li F, Min Y, Zhang Y, Zhang Y, Zuo H, Bai F. Evaluation method for consistency of lithium-ion battery packs in electric vehicles based on the Mahalanobis-Taguchi system. J Energy Storage 2024;78.
[39] Liu Q, Ma J, Zhao X, Zhang K, Xiangli K, Meng D. A novel method for fault diagnosis and type identification of cell voltage inconsistency in electric vehicles using weighted Euclidean distance evaluation and statistical analysis. Energy 2024;293.
[40] Wang L, Hu Z, Tian A, Chang C, Wu M. An inconsistency fault diagnosis method for lithium-ion cells in the battery pack based on piecewise dimensionality reduction and outlier identification. J Electrochem Energy 2023;20(1).
[41] Li D, Deng J, Zhang Z, Liu P, Wang Z. Multi-dimension statistical analysis and selection of safety-representing features for battery pack in real-world electric vehicles. Appl Energy 2023;343.
[42] Liu Q, Ma J, Zhao X, Zhang K, Meng D. Online diagnosis and prediction of power battery voltage comprehensive faults for electric vehicles based on multi-parameter characterization and improved K-means method. Energy 2023;283.
[43] Zhang H, Li S, Chen F, Pan X, Feng H, Sun Y. Battery voltage fault diagnosis for electric vehicles considering driving condition variation. IET Intell Transp Syst 2024;18(4):574-590.
[44] Zhang X, Yang W, Yan L, Kaleem M B, Liu W. Adaptive internal short-circuit fault detection for lithium-ion batteries of electric vehicles. J Energy Storage 2024;84.
[45] Huang R, Peng Y, Yang J, Xu X, Deng P. Correlation analysis and prediction of PEM fuel cell voltage during start-stop operation based on real-world driving data. Energy 2022;260.
[46] Zhao H, Chen Z, Shu X, Shen J, Liu Y, Zhang Y. Multi-step ahead voltage prediction and voltage fault diagnosis based on gated recurrent unit neural network and incremental training. Energy 2023;266.
[47] Hong J, Wang Z, Yao Y. Fault prognosis of battery system based on accurate voltage abnormity prognosis using long short-term memory neural networks. Appl Energy 2019;251.
[48] Li D, Zhang Z, Liu P, Wang Z, Zhang L. Battery Fault Diagnosis for Electric Vehicles Based on Voltage Abnormality by Combining the Long Short-Term Memory Neural Network and the Equivalent Circuit Model. IEEE Trans Power Electron 2021;36(2):1303-15.
[49] Xu G, Han Q, Chen H, Xia Y, Liu Z, Tian S. Safety warning analysis for power battery packs in electric vehicles with running data. J Energy Storage 2022;56:105878.
[50] Breiman L. Random forests. Mach Learn 2001;45(1):5-32.
[51] Friedman J. Greedy function approximation: a gradient boosting machine. Ann Statist 2001;29(5):1189-232.
[52] Apley D, Zhu J. Visualizing the effects of predictor variables in black box supervised learning models. J R Stat Soc B 2020;82(4):1059-1086.

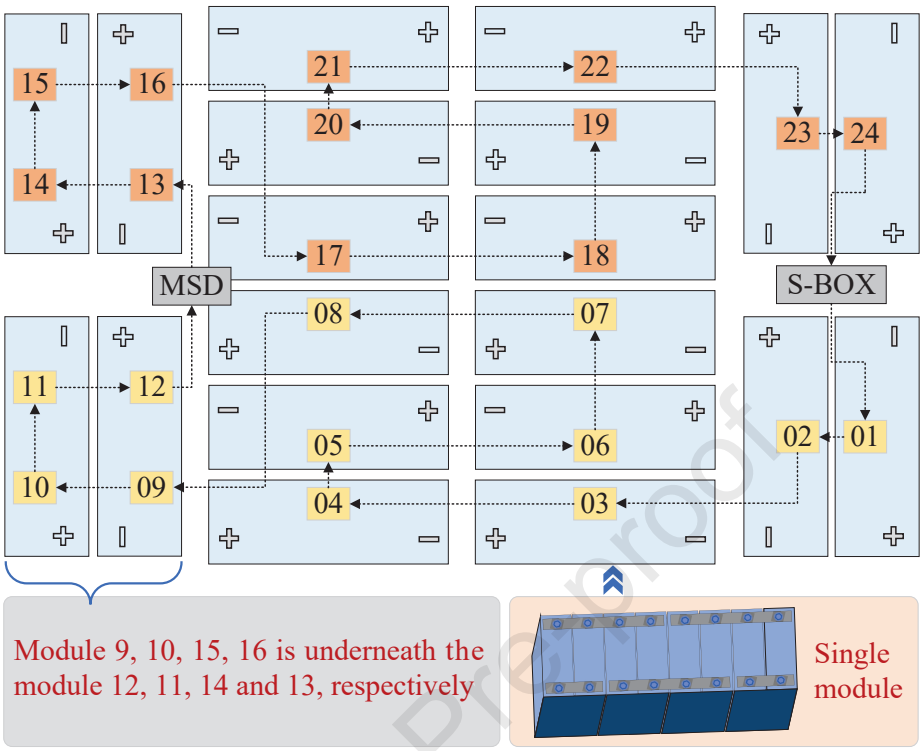

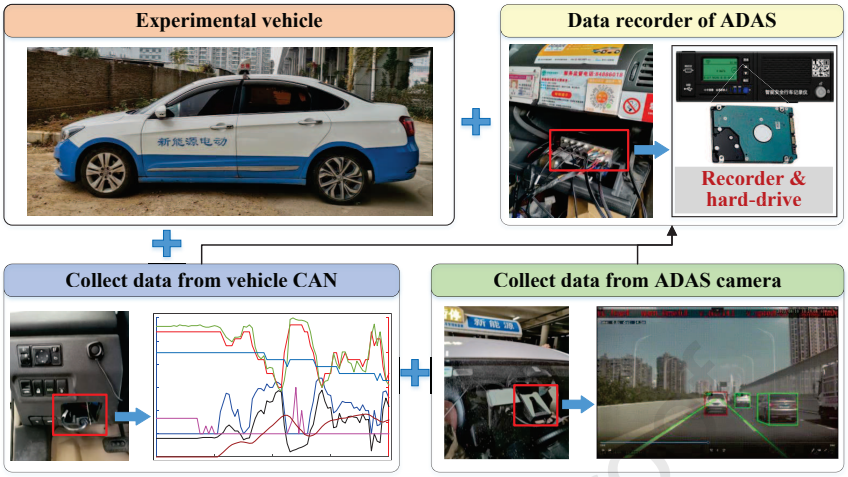

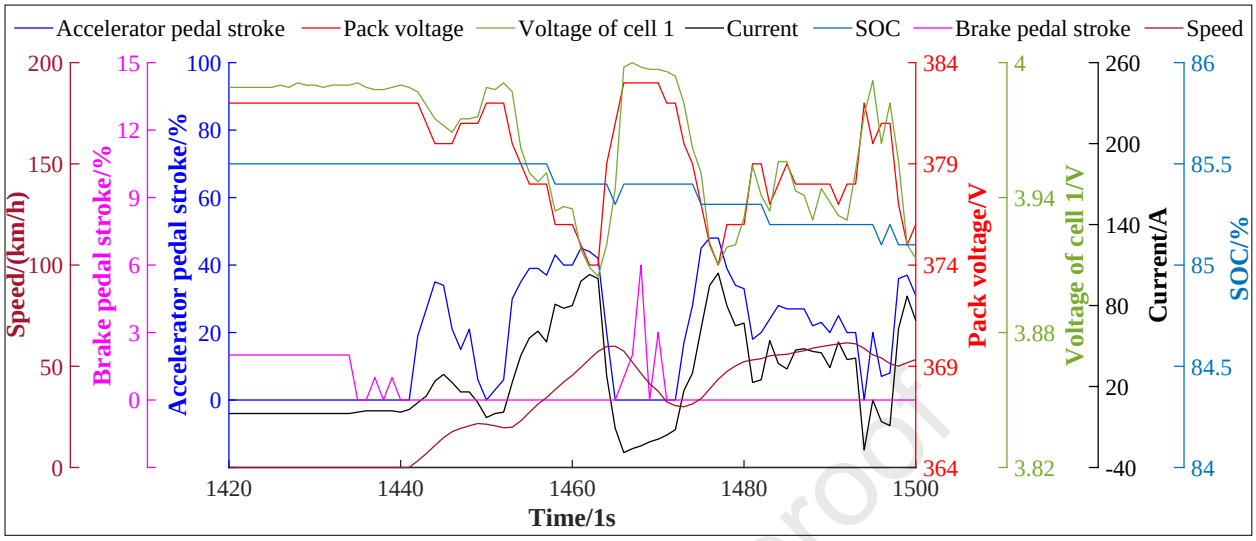

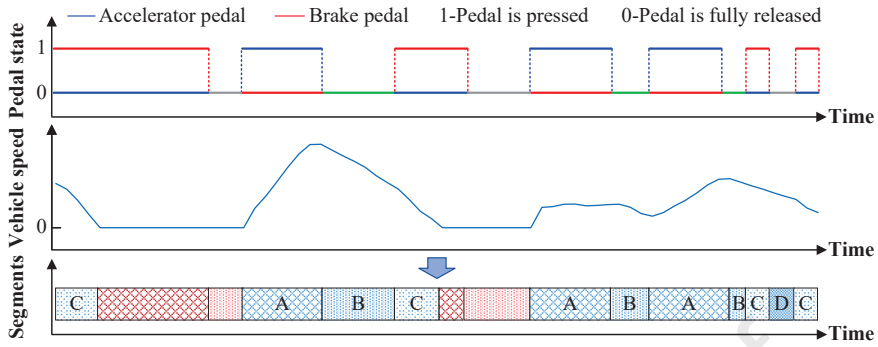

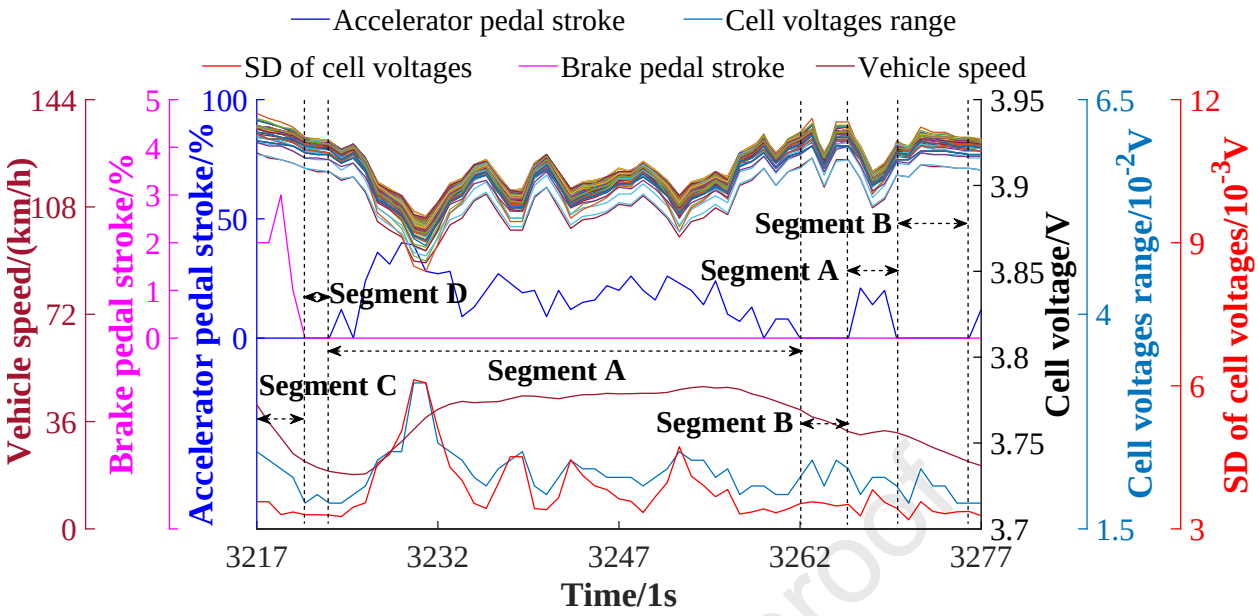

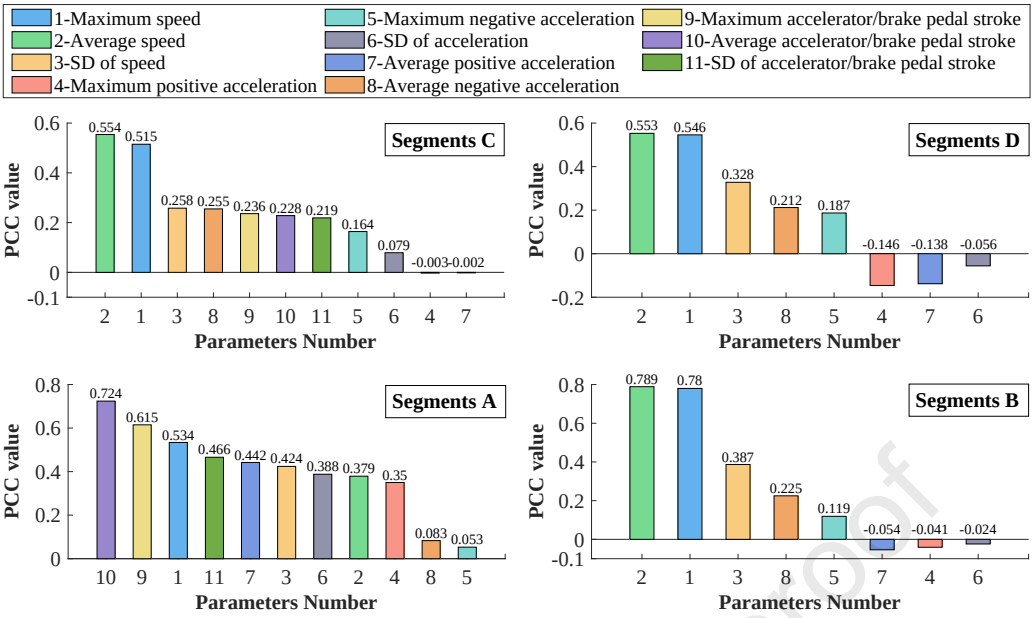

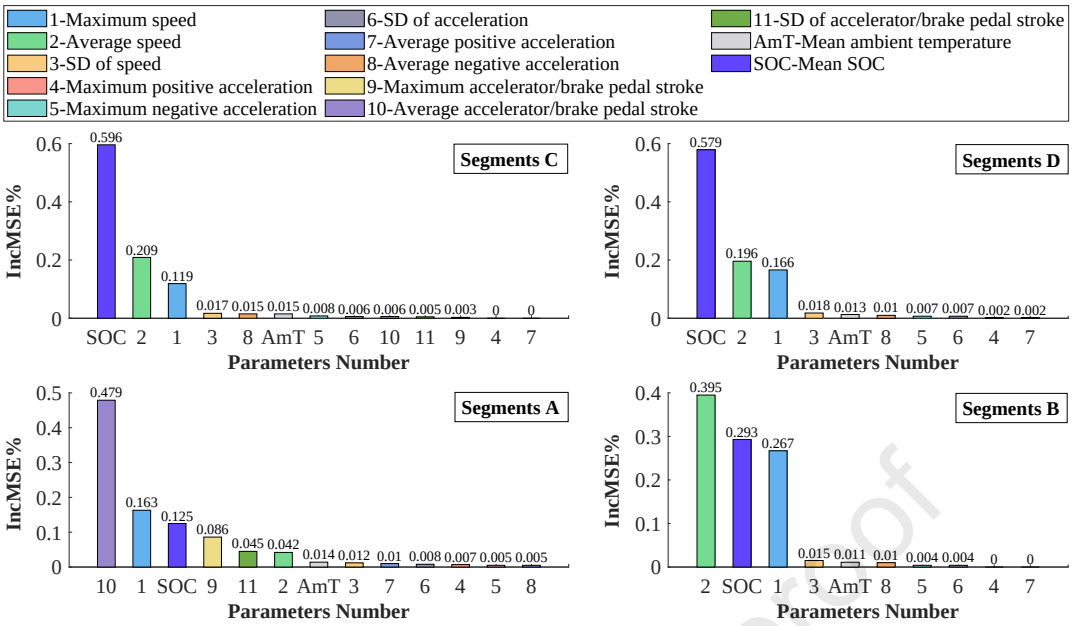

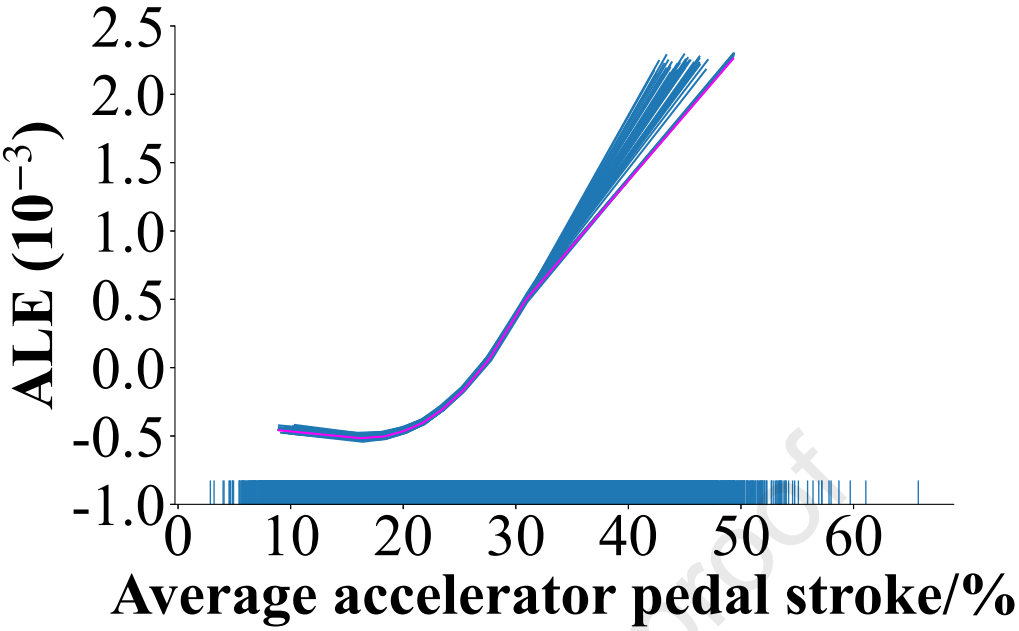

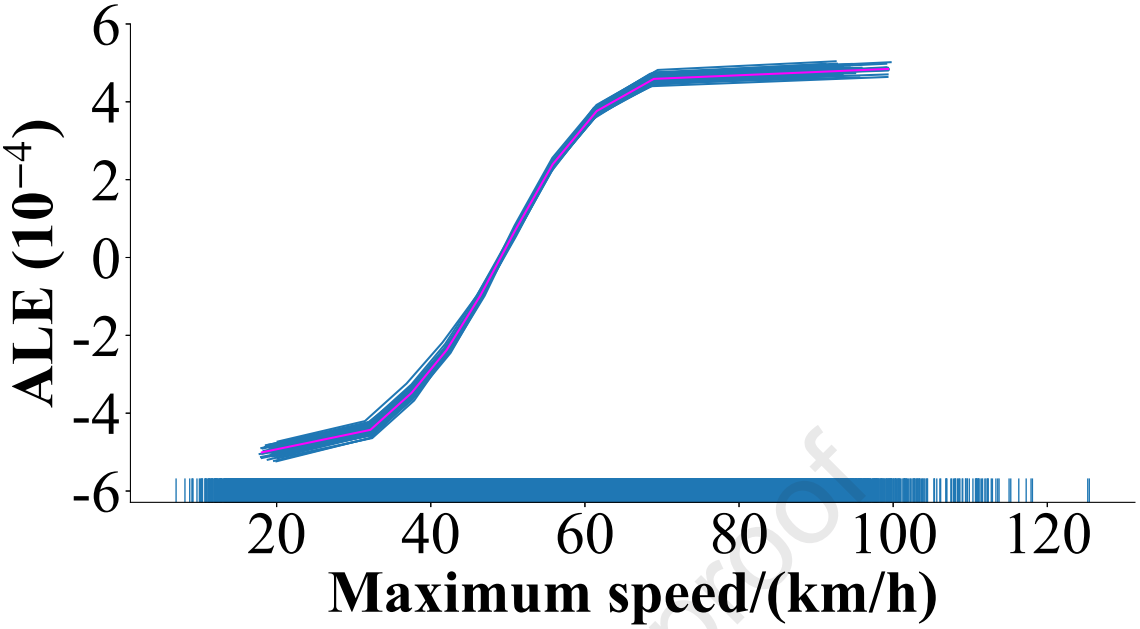

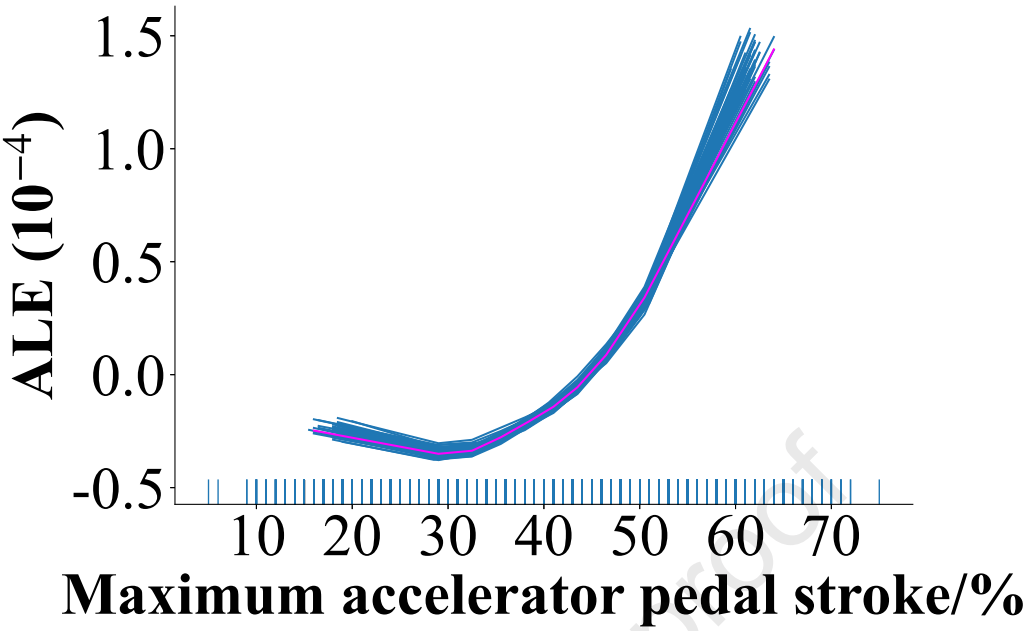

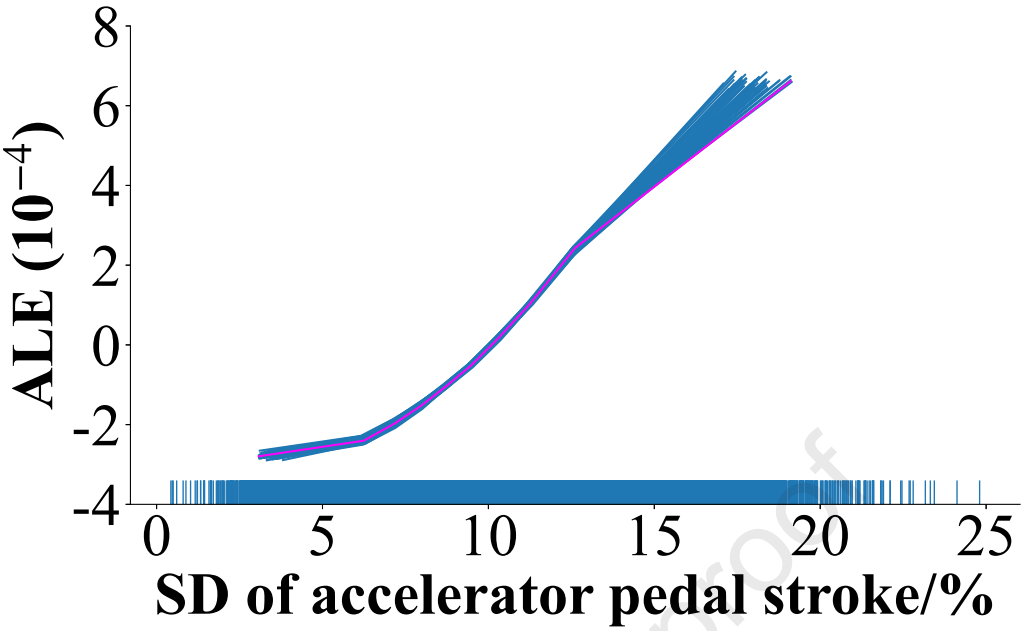

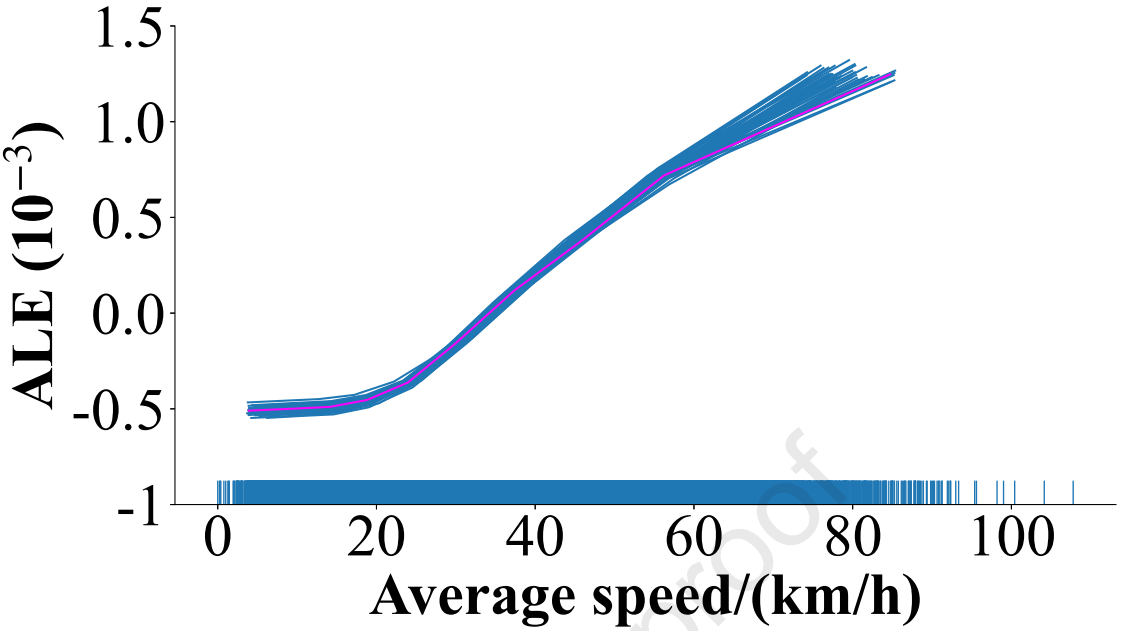

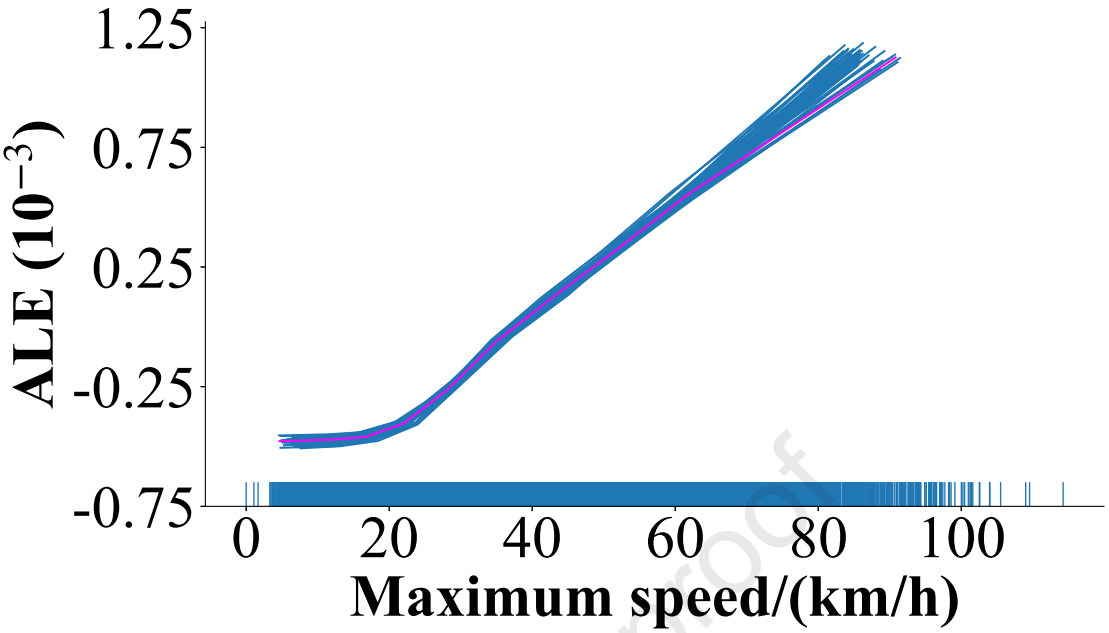

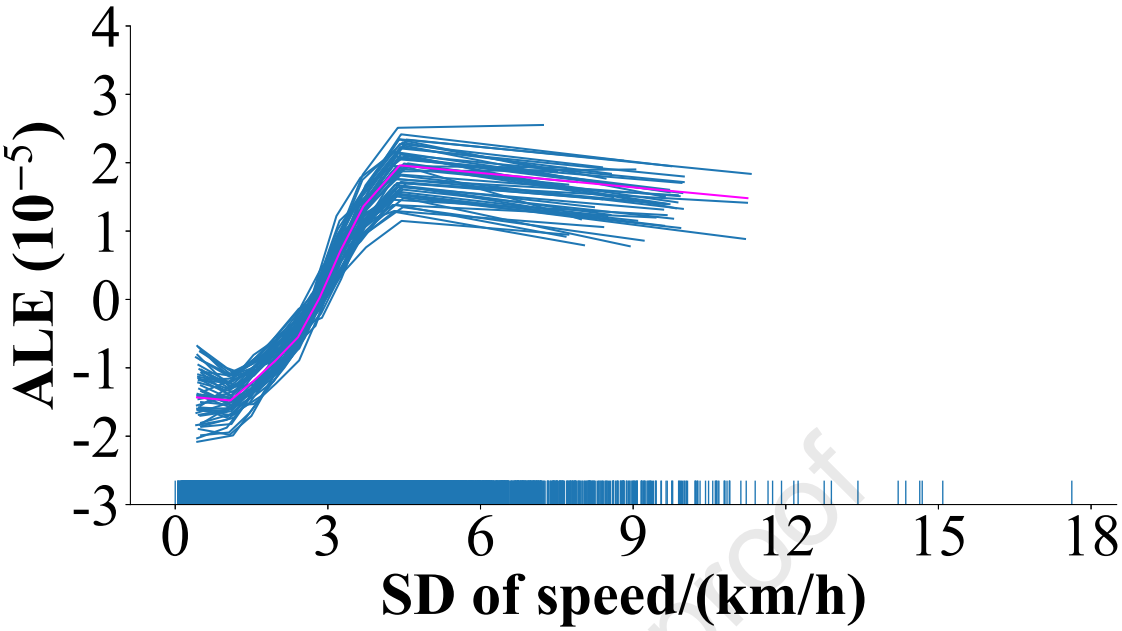

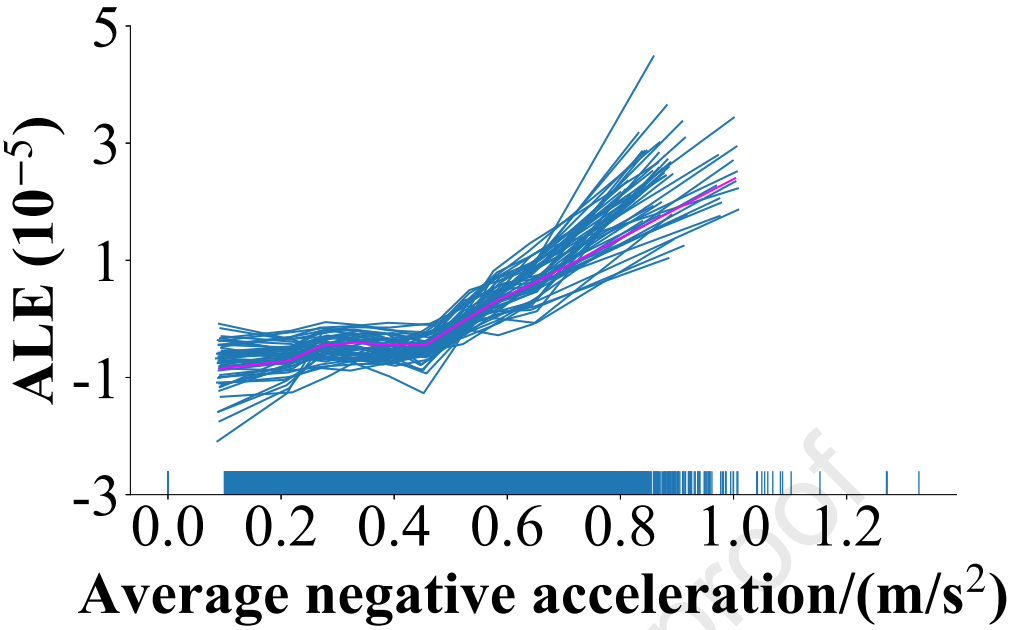

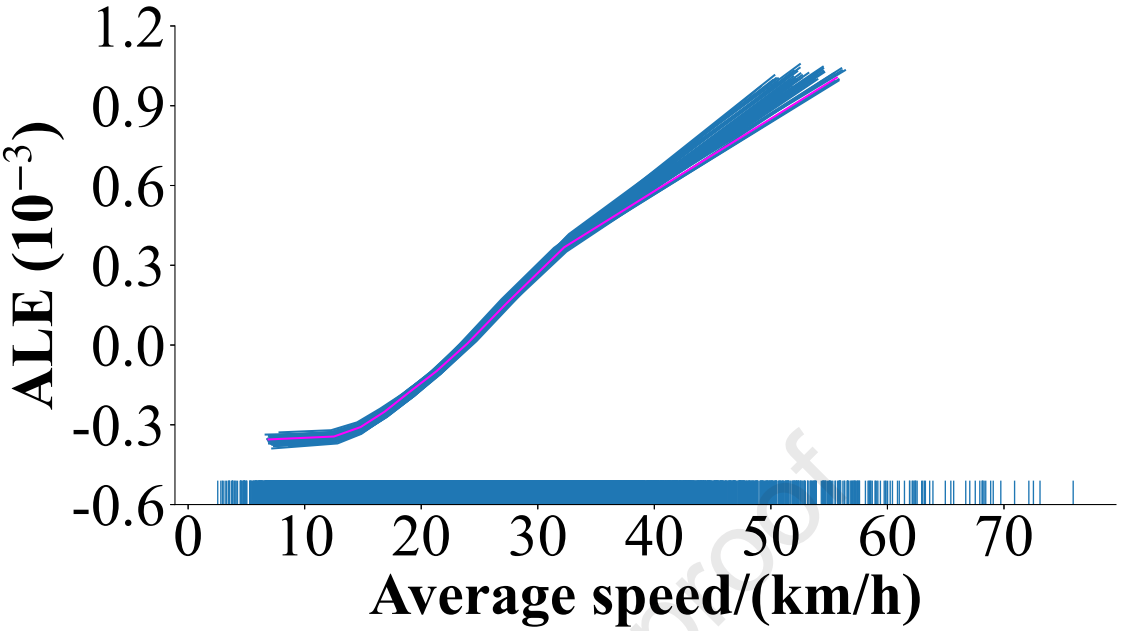

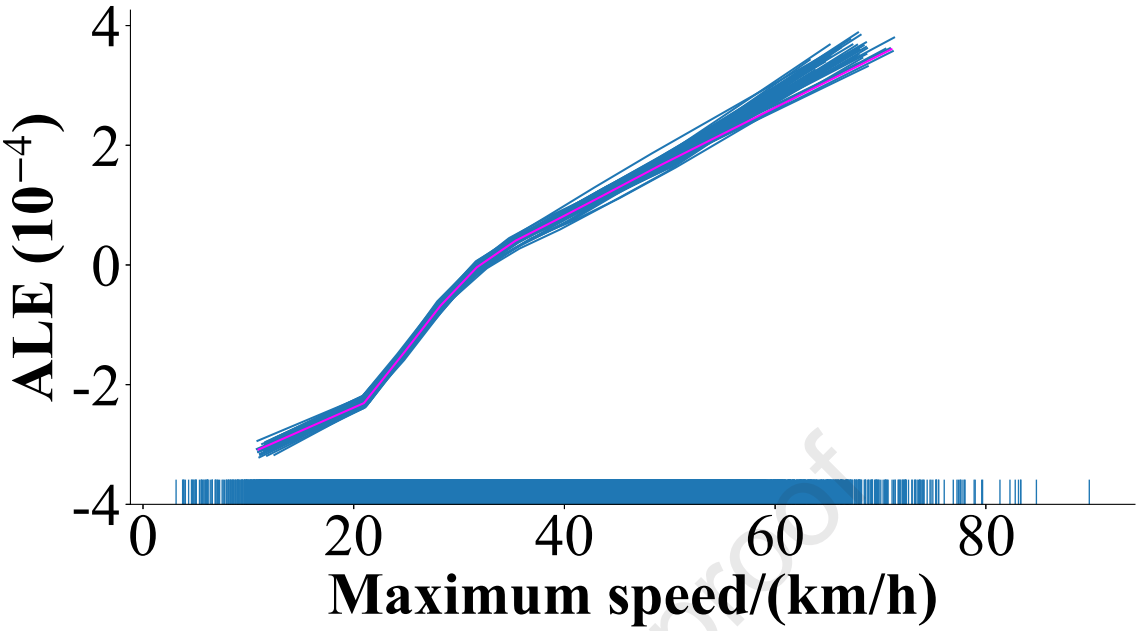

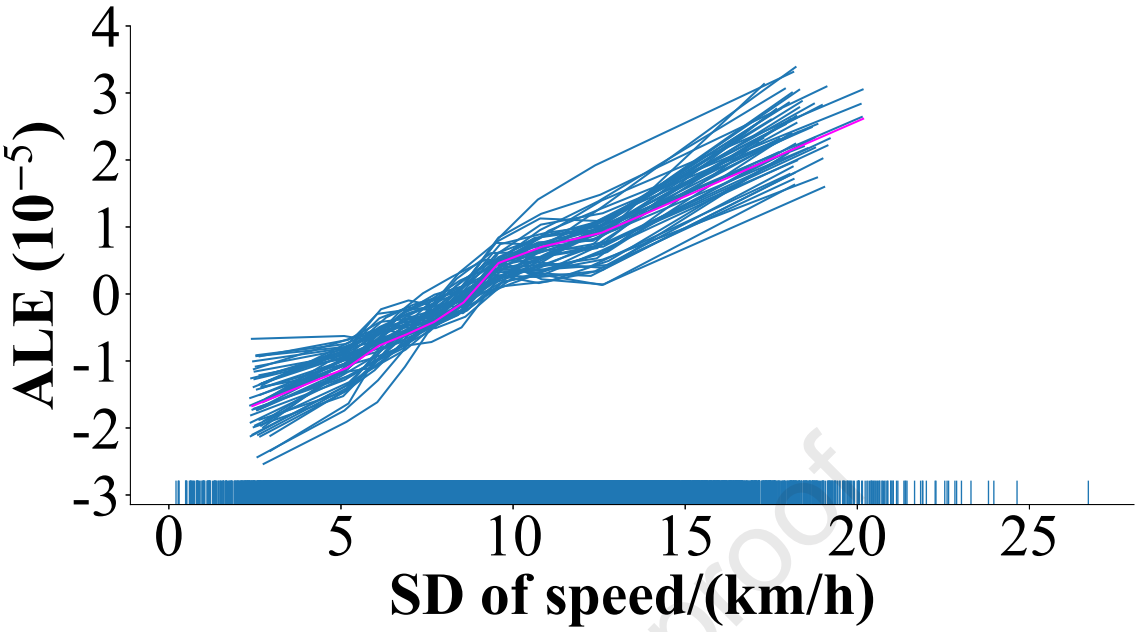

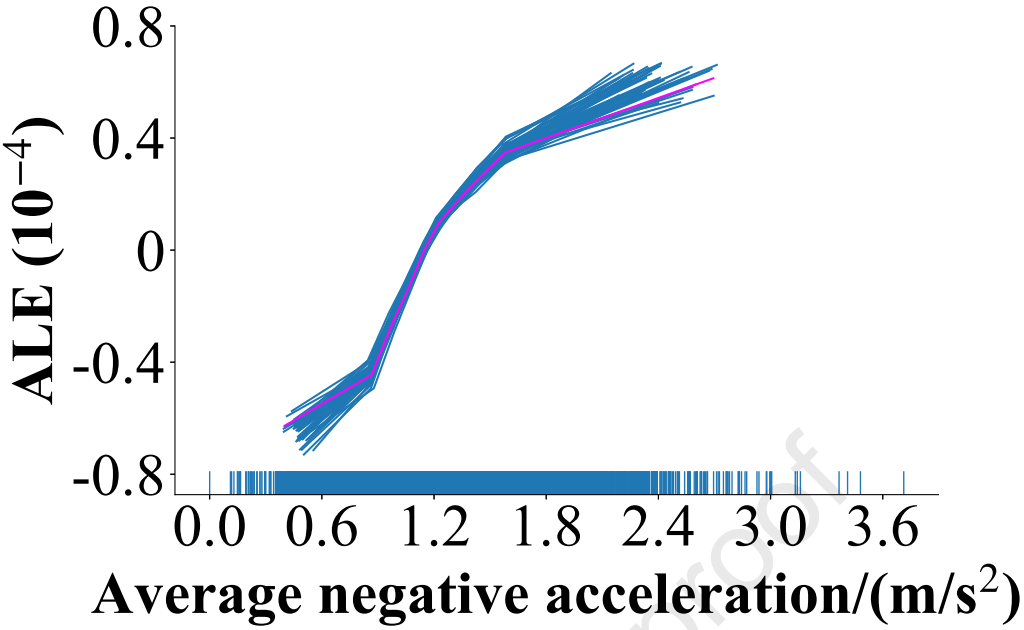

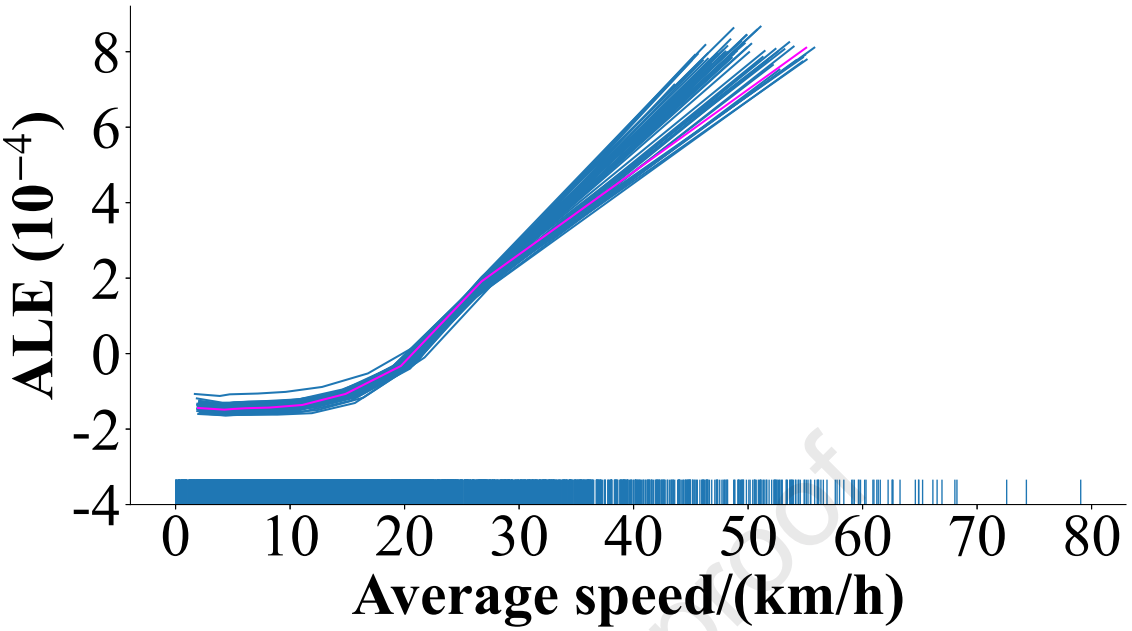

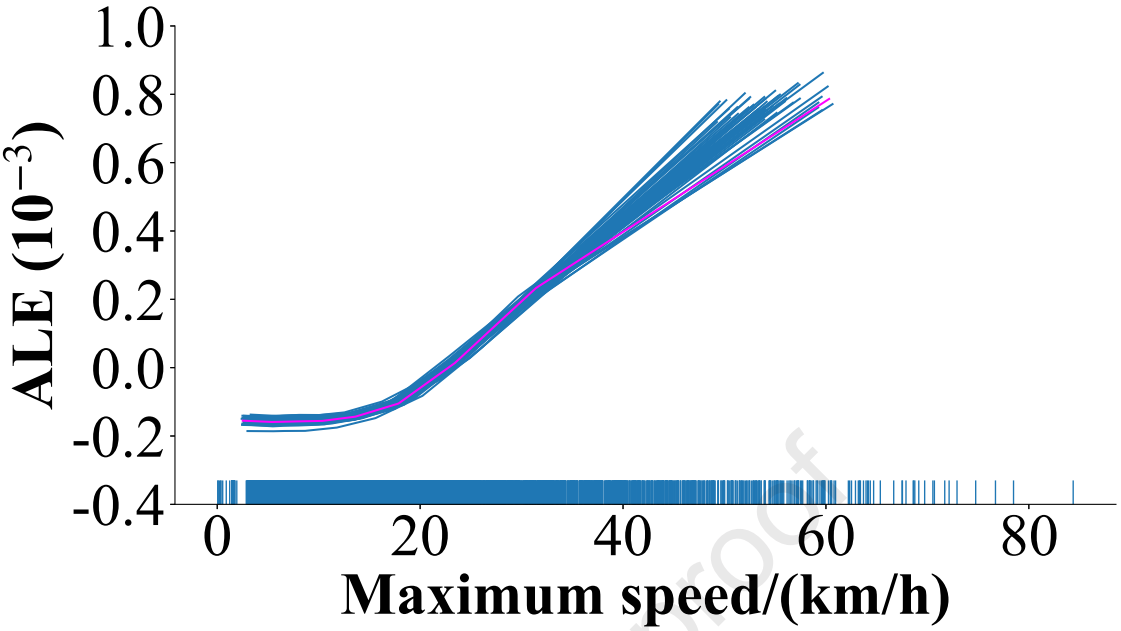

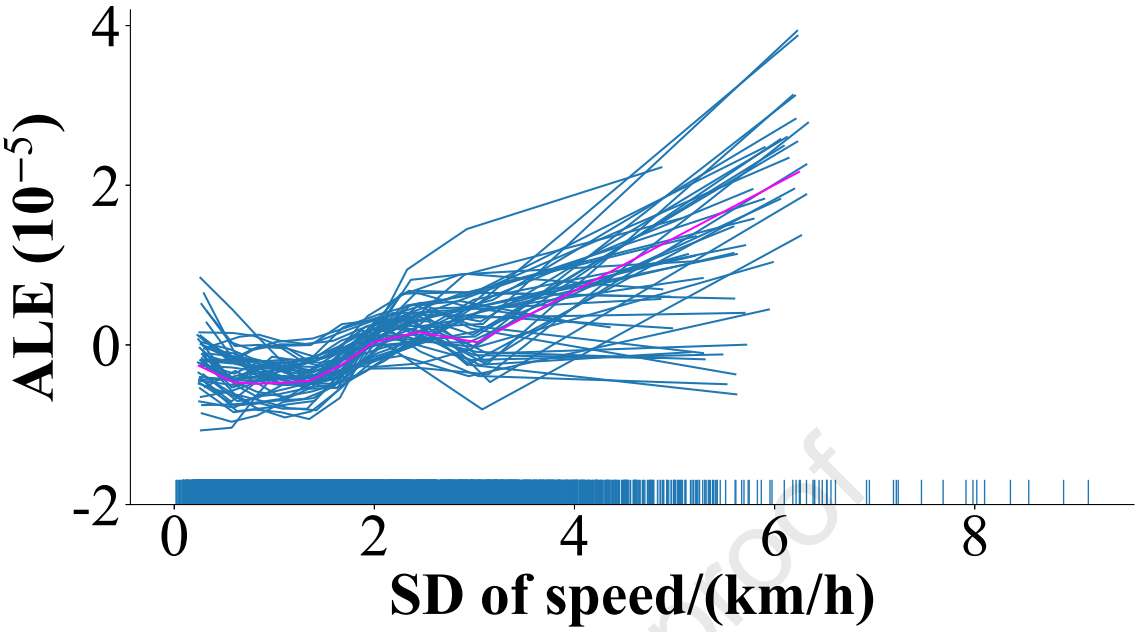

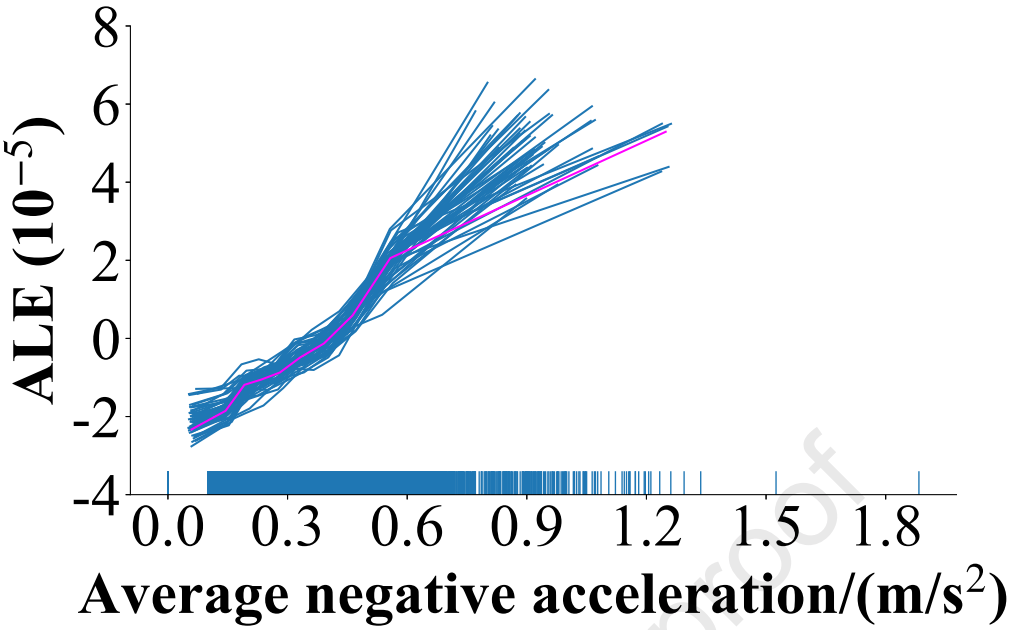

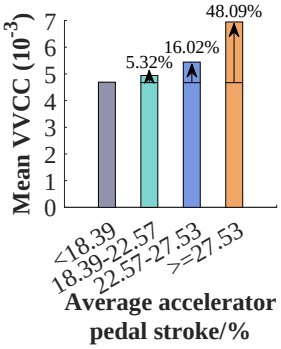

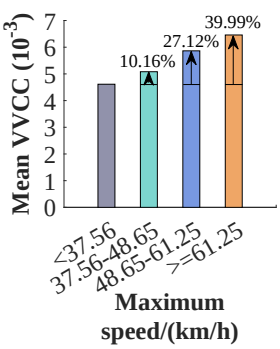

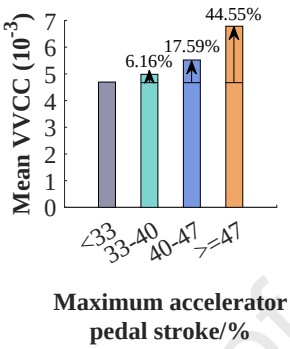

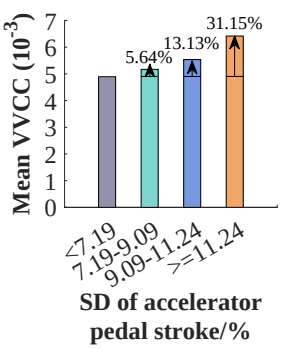

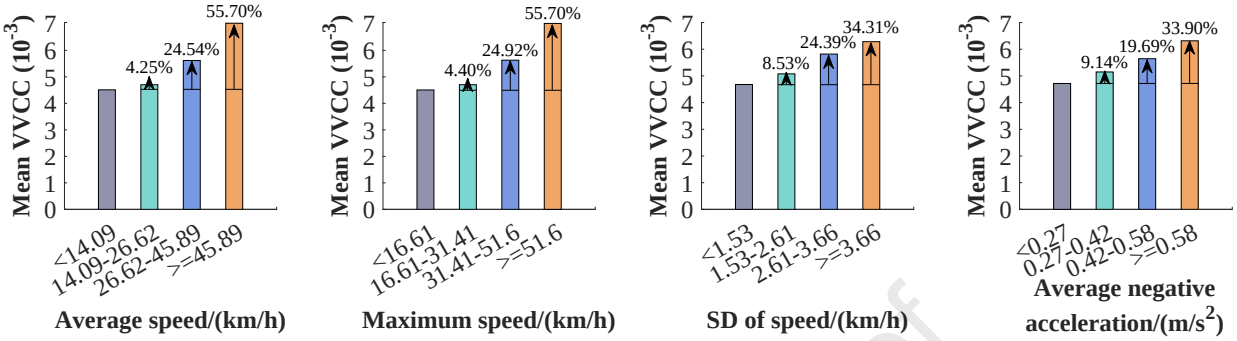

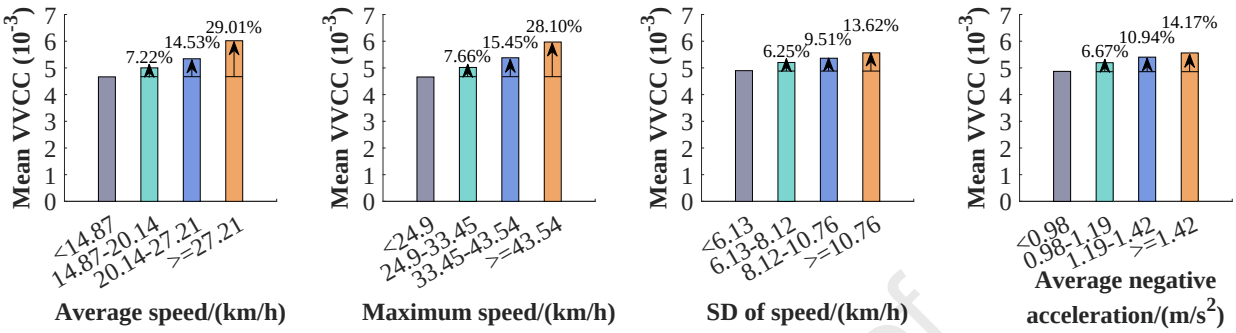

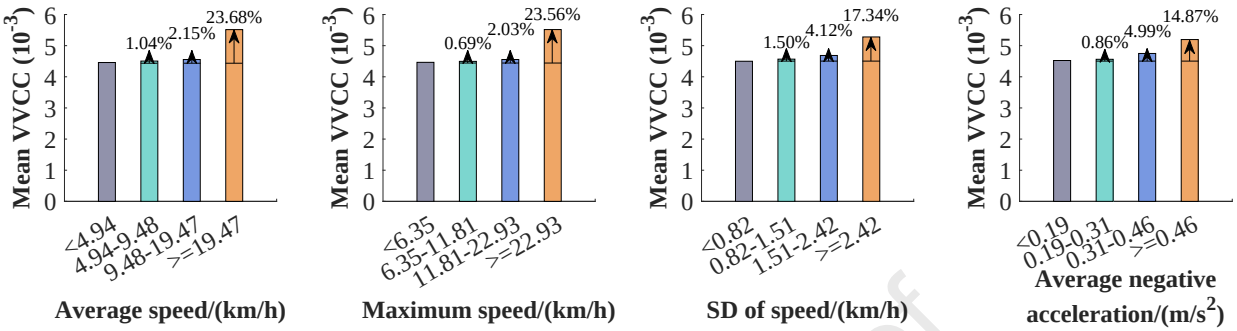

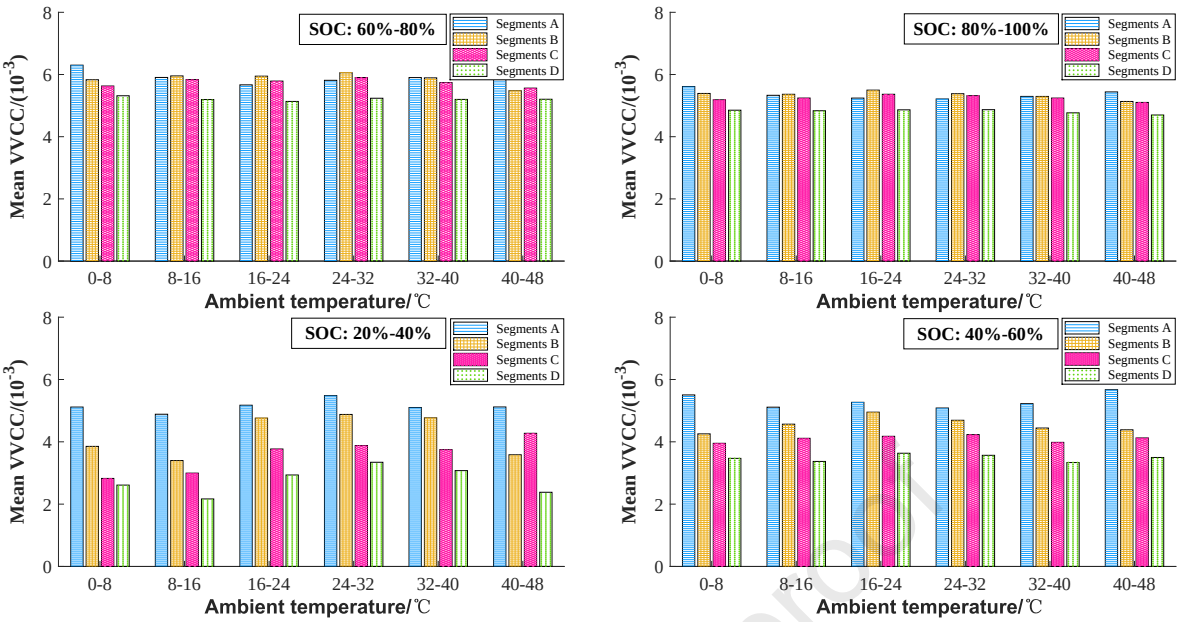

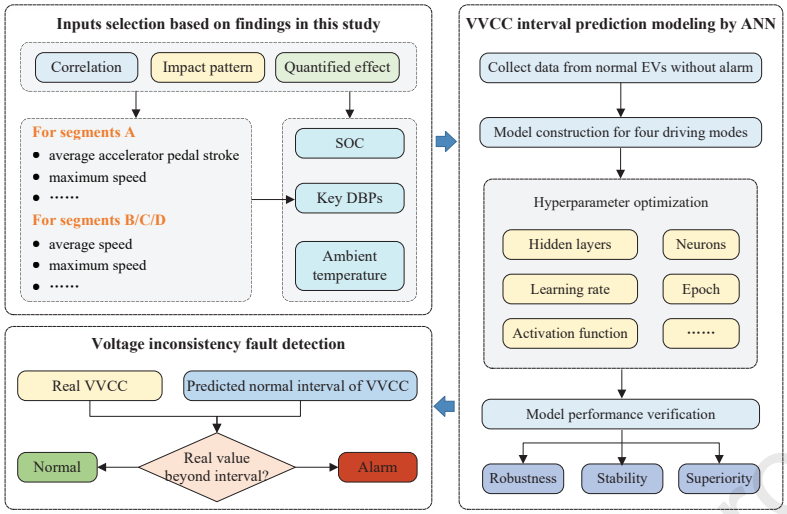

HIGHLIGHTS

- Naturalistic driving experiment is conducted to collect running data from actual electric vehicles
- Relationship between driving behavior and voltage consistency is investigated
- Pearson correlation coefficients between driving behavior and cell voltage consistency are calculated
- Accumulated local effects of driving behavior parameters on cell voltage consistency are obtained using random forest models

Declaration of competing interest

The authors declare that they have no known competing financial interests or personal relationships that could have appeared to influence the work reported in this paper.